LLNL-JRNL-835203

Replicating HCCI-like Autoignition Behavior: What Gasoline Surrogate Fidelity is Needed?

S. Cheng, S. Scott Goldsborough, S. W. Wagnon, R. Whitesides, M. McNenly, W. J. Pitz, D. Lopez-Pintor, J. E. Dec

May 12, 2022

Applications in Energy and Combustion Science

Replicating HCCI-like autoignition behavior: what gasoline surrogate fidelity is needed?

Song Cheng[1,2,6,*], S. Scott Goldsborough[1,*], Scott W. Wagnon[3], Russell Whitesides[4], Matthew McNenly[4], William J. Pitz[3], Dario Lopez-Pintor[5], John E Dec[5]

[1]Energy System Division, Argonne National Laboratory, Lemont, IL 60439, USA

[2]Department of Mechanical Engineering, The Hong Kong Polytechnic University, Kowloon, Hong Kong

[3]Materials Science Division, Lawrence Livermore National Laboratory, Livermore, CA 94551, USA

[4]Computational Engineering Division, Lawrence Livermore National Laboratory, Livermore, CA 94551, USA

[5]Combustion Research Facility, Sandia National Laboratories, Livermore, CA 94550, USA

[6]Research Institute for Smart Energy, The Hong Kong Polytechnic University, Kowloon, Hong Kong

[*] Corresponding Authors:

Song Cheng
+852-2766-6668
songryan.cheng@polyu.edu.hk

S. Scott Goldsborough
+1-630-252-9375
scott.goldsborough@anl.gov

ABSTRACT

This work seeks to characterize the fidelity needed in a gasoline surrogate with the intent to replicate the complex autoignition behavior exhibited within advanced combustion engines, and specifically Homogeneous Charge Compression Ignition (HCCI). A low-temperature gasoline combustion (LGTC) engine operating in HCCI mode and a rapid compression machine (RCM) are utilized to experimentally quantify fuel reactivity, through autoignition and preliminary heat release characteristics. Fuels considered include a research grade E10 U.S. gasoline (RD5-87), three multi-component surrogates (PACE-1, PACE-8, PACE-20), and a binary surrogate (PRF88.4). Each fuel was studied at lean/HCCI-like conditions covering a wide range of temperatures and pressures that are representative of naturally aspirated to high boost engine operation. Detailed chemical kinetic modeling is also undertaken using a recently updated gasoline surrogate kinetic model to simulate the RCM experiments and to provide chemical insight into surrogate-to-surrogate differences.

The LGTC engine experiments demonstrate nearly identical reactivity between PACE-20 and RD5-87 across conditions, while faster phasing is seen for both PACE-1 and PACE-8 due to their stronger intermediate- and low-temperature heat release (ITHR/LTHR) at naturally aspirated and boosted conditions, respectively. The RCM experiments reveal typical low-temperature, negative temperature coefficient (NTC) and intermediate-temperature autoignition behaviors at all pressure conditions for RD5-87, which are qualitatively reproduced by all surrogates. Quantitative discrepancies in both autoignition and preliminary heat release are observed for all surrogates, while their ability to replicate RD5-87 autoignition behavior follows the order of PACE-20 > PACE-1 > PACE-8 > PRF88.4. Excellent mapping is obtained between the LGTC engine and the RCM, where the engine pressure-time trajectories can be characterized by the regimes represented by the RCM autoignition isopleths. The kinetic model performs commendably when simulating both autoignition and preliminary heat release of PACE-20, while typically overpredicting ignition delay times for PACE-1, PACE-8 and PRF88.4 at high-pressure and low-temperature/NTC conditions. Sensitivity and rate of production (ROP) analyses highlight surrogate-to-surrogate differences in the governing chemical kinetics where *n*-pentane initiates rapid OH branching at a faster rate and an earlier timing for PACE-20, making it computationally more reactive than the other surrogates. The current study highlights the need to include non-standardized properties, such as the lean/HCCI-like autoignition characteristics, in addition to ASTM properties (e.g., RON, MON) as metrics of fuel reactivity and targets to be matched when formulating high-fidelity surrogates that fully capture gasoline advanced combustion behavior such as HCCI-like autoignition.

Keywords: low temperature gasoline combustion engine, rapid compression machine, HCCI-like autoignition, gasoline surrogates, chemical kinetic modeling

1. INTRODUCTION

Petroleum-derived, full-boiling-range gasolines are currently the most widely used transportation fuel, powering over 50% of all existing passenger cars [1]. In recent years, the growing demand toward cleaner combustion and higher efficiency has pushed the development of new gasoline fuels that can be co-optimized with advanced engine systems. This requires a thorough understanding of gasoline combustion characteristics at various operating conditions, which is challenging given that petroleum-derived gasolines vary in compositions and properties. Better and consistent insight can be gained by using gasoline surrogates with significantly fewer and invariant components that are able to reproduce a range of chemical and physical properties of complex gasolines. The use of gasoline surrogates also makes modeling and simulation tenable and limiting the diversity of the fuel components can considerably reduce the number of species that need to be represented in models, enabling computational fluid dynamic (CFD) simulation of practical combustors and development of chemical kinetic models that are beneficial for engineering design. This is also true for the aviation sector where pursuits for higher efficiencies and lower criteria and greenhouse gas emissions have driven the design of new combustors and alternative fuels.

The formulation of gasoline surrogate fuels has already been investigated for many years [2, 3]. Historically, binary blends of *n*-heptane and *iso*-octane, termed primary reference fuels (PRF), have been used as the simplest gasoline surrogates motivated by their use in octane ratings in the standardized American Society for Testing and Materials (ASTM) tests for research octane number (RON) [4] and motor octane number (MON) [5]. Ternary blends of *n*-heptane, *iso*-octane and toluene (known as toluene primary reference fuels (TPRF)) have also been used as gasoline surrogates to be able to match octane sensitivity (RON minus MON, denoted as S) [6, 7]. However, the growing need to better understand and model the complex underlying chemistry of gasoline combustion requires surrogates to capture additional properties beyond octane numbers, including hydrogen to carbon ratio (H:C) [8-10], PIONA (paraffins, iso-paraffins, olefins, naphthenes, and aromatics) compositions [8-10], individual carbon bonding types [10], distillation curve/volatility [10, 11], etc. These additional properties cannot be adequately replicated by simple surrogates such as PRFs and TRFs, and require use of multi-component surrogate formulations [12-14].

Fuel reactivity is one of the most important fuel properties for surrogates to replicate, as autoignition behavior controls combustion phasing in low temperature combustion (LTC) conditions and engine knock in spark-ignited conditions. The selection of target properties to represent fuel reactivity is often linked closely to the engine application in which the gasoline fuel is used. In spark-ignition (SI) engines, fuel reactivity is represented by antiknock quality, which is determined by the ability of the fuel to resist end-gas autoignition from piston and flame compression. The most popular target properties to represent fuel anti-knock quality have been RON and MON for conventional SI engines [4, 5], and octane index (OI) and *K* values (OI = RON – K*S) for modern direct injection spark ignition (DISI) engines [15]. On the other hand, gasoline fuels can also be used in LTC engines with HCCI (homogeneous charge compression ignition), PPC (partially premixed combustion) and GCI (gasoline compression ignition) operating strategies. LTC engines have been attractive, demonstrating many benefits in comparison to conventional SI and compression-ignition (CI) engines, such as combining the low soot emissions of SI engines and the high thermal efficiency of diesel engines. The combustion process in LTC engines also differs notably from SI engines, where an appropriate autoignition reactivity is sought, to obtain the desired onset of heat release and combustion phasing. Properly replicating gasoline autoignition behavior in LTC engines can be more challenging than in SI engines, as the autoignition process in LTC engines progresses mostly in the low-temperature regime, which deviates from the temperature conditions experienced by the end-gas in standard RON and MON tests. Efforts have been addressed to develop new ignition quality metric for LTC engines, such as the autoignition temperature metric developed by Truedsson et al. [16-18], the revised octane index proposed by Lacey et al [19], and, most practically, the 10% mass fraction burned (CA10) and 50% mass fraction burned (CA50) [3] that are commonly used for LTC engine control. Despite these metrics, almost all gasoline surrogates for LTC engines are still formulated using RON, MON and S as target properties to represent fuel autoignition reactivity [2]. Another important fuel behavior in LTC engines is the low temperature heat release (LTHR), which plays a critical role in determining the overall gasoline autoignition characteristics. For instance, in PPC/GCI combustion, LTHR can lead to the generation of low-temperature ignition kernels and fronts, which subsequently affect the generation of high-temperature ignition kernels [20]; in HCCI combustion, LTHR at early stages of combustion process can considerably advance combustion phasing [13]. Despite the importance of LTHR, it has rarely been considered as a target property for the formulation of gasoline surrogates [2]. Both the end-gas autoignition in SI engines and LTHR characteristics in LTC engines, particularly HCCI engines, are primarily governed by the underlying oxidation chemistry. Therefore, the oxidation chemistry of the full boiling range gasolines should be sufficiently matched by the surrogate fuel at relevant conditions, to adequately represent these important behaviors.

As a target gasoline, the current study focuses on a research-grade E10 gasoline (RD5-87), which was developed to represent typical regular-grade E10 market gasoline in the U.S. The use of RD5-87 facilitates consistency and collaboration across different research groups in the Partnership for Advanced Combustion Engines (PACE) consortium [21]. As part of the PACE collaboration, multi-component surrogates including PACE-1, PACE-8 and PACE-20 (each discussed in more details in Section 2) were developed out of an effort to recommend a surrogate fuel that best matches the properties and measurements of RD5-87 [22].

Combustion characteristics of RD5-87 have been experimentally investigated in a low-temperature gasoline combustion (LTGC) engine [23-26], a gasoline direct injection spark-ignition (DISI) engine [27], an EGR-diluted DISI engine [28, 29], a Cooperative Fuel Research engine [30], several light-duty diesel engines [30], and a heavy-duty diesel engine [31]. These studies provided useful characterization of system-level and end-use performance of RD5-87 under practical engine conditions. Modeling-wise, Cuoci et al. [32] simulated the soot formation characteristics of a seven-component surrogate for RD5-87 using a detailed chemical kinetic model and a soot model. Comparison with the experiments was also carried out, with reasonable qualitative agreement but obvious quantitative disagreement obtained. Following this, Pal and co-workers [33] performed 3-D CFD simulations of a single cylinder gasoline compression ignition engine to investigate the impact of oxygenated blending on RD5-87 soot emissions under low load conditions. A four-component fuel (TRF with ethanol) in conjunction with a skeletal chemical kinetic model were used to represent RD5-87 and to reduce the computational cost in the CFD simulation. They found that fuel autoignition propensity was primarily dictated by fuel chemistry, which showed strong coupling with sooting propensity. Guleria et al. [34] compared three gasoline skeletal models under partial fuel stratification in an LTGC engine using a 3-D CFD model with large eddy simulations, where the simulation results showed discrepancies with the experiments for RD5-87. For these modeling studies, since comparison was made between the model and the experiments for RD5-87, it is unclear if the discrepancies between model and experiments were caused by insufficiency in the surrogate makeup or the selected chemical kinetic models. On the other hand, only limited efforts have been made to establish direct, experimental comparison between RD5-87 and it surrogates. Szybist investigated the effectiveness of EGR to mitigate knock in a DISI engine [28], where RD5-87 was compared to PACE-1, and differences in measured cylinder pressure-time histories were highlighted. The emissions of NO, acetylene, ethylene and formaldehyde were also recorded at various conditions, providing evaluable data for kinetic model validation. Very recently, Wan et al. [35] compared the soot and PAH formation in high-pressure spray pyrolysis of RD5-87 with those of PACE-8 and PACE-20. Good agreement was observed for both surrogates with better agreement observed for PACE-20 than for PACE-8.

The objectives of this work are to: 1) understand the surrogate fidelity that’s required to adequately replicate gasoline autoignition at HCCI-like conditions, through direct comparisons in the autoignition (timing) and preliminary heat release characteristics between RD5-87 and a range of surrogates that are formulated targeting different RD5-87 properties; 2) quantify the surrogate-to-surrogate differences in autoignition (timing) and preliminary heat release characteristics, as well as the governing chemical kinetics; and 3) provide fundamental autoignition data that are valuable for model verification and validation, thereby facilitating accurate chemical kinetic models to aid the design of high-fidelity combustion engine simulations. HCCI-like conditions are selected since the autoignition and preliminary heat release behavior in HCCI engines are less affected by gas mixing effects, hence easier to interpret in comparison to other LTC engines such as PPC engines. Toward this, new measurements are conducted for RD5-87 and four surrogates (PACE-1, PACE-8, PACE-20 and PRF88.4) using an LTGC engine and a rapid compression machine (RCM) at lean/HCCI-like conditions across a wide range of temperatures and pressures representative of naturally aspirated to high boosted engine operations. Changes in overall reactivity and heat release behavior are quantified at different conditions and compared across the surrogate fuels to evaluate their ability in replicating RD5-87. A recently-updated, detailed gasoline surrogate model is also used to simulate the RCM experiments, providing chemical insight into the surrogate-to-surrogate differences.

The remaining manuscript is organized as follows. Section 2 provides a description of the experimental facilities used for data acquisition as well as methods used for post-processing. Section 3 outlines the details of the chemical kinetic modeling. Section 4 discusses the experimental and modeling results. This is followed by a summary of the paper in Section 5.

2. EXPERIMENTAL

2.1. Gasoline and surrogate formulation

2.1.1. Gasoline

A research-grade, full-boiling-range E10 (10% liquid volume ethanol) gasoline with antiknock index (AKI) of 88.4, termed RD5-87, was used in this study. The PIONA-X distribution and some key properties of RD5-87 can be found in Tables 1 and 2, respectively.

Table 1. Composition of RD5-87, PACE-1 PACE-8, PACE-20 and PRF88.4, liquid volume basis.

Hydrocarbon Class	RD5-87	Palette Compound	RD5-87*	PACE-1	PACE-8	PACE-20	PRF88.4
n-**P**araffins	16.8	*n*-Pentane	8.8	-	-	14.0	-
		n-Heptane	<0.1	18.7	16.8	11.5	11.6
***I**so*-paraffins	32.8	2-Methyl butane	<0.1	7.7	10.4	-	-
		Iso-octane	13.2	21.4	24.5	25.0	88.4
Olefins	6.7	1-Hexene	4.7	6.6	5.4	5.4	-
Naphthenes	11.5	Cyclopentane	5.9	10.5	8.3	10.5	-
Aromatics	22.1	Toluene	7.6	-	-	9.2	-
		1,2,4-Trimethylbenzene	1.9	25.7	25.2	11.9	-
		Tetralin	-	-	-	3.0	-
o**X**ygenates	10.1	Ethanol	9.1	9.4	9.4	9.6	-

*concentrations determined from detailed hydrocarbon analysis.

Table 1. Select properties of RD5-87 and its surrogates: PACE-1, PACE-8, PACE-20 and PRF88.4.

Properties	RD5-87	PACE-1	PACE-8	PACE-20	PRF88.4
RON[a]	92.3	91.8	92.2	92.1	88.4
MON[a]	84.6	82.3	84.2	84.5	88.4
AKI[b]	88.4	87.0	88.2	88.3	88.4
S[b]	7.7	9.5	8.0	7.6	0.0
H/C ratio	1.969	1.970	1.981	1.964	2.254
Density at 15 °C [g/cc]	0.750	0.745	0.742	0.742	0.699
LHV [MJ/kg]	41.770	41.706	41.706	41.705	44.681
PMI	1.68	1.56	1.54	1.50	-
T10 [°C] [c]	57.8	60.4	59.6	57.9	-
T50 [°C] [c]	101.3	100.6	102.9	89.9	-
T90 [°C] [c]	157.9	165.8	165.6	166.0	-
final boiling point [°C][c]	205.0	166.6	176	193.8	-

[a] Measured in this work by ASTM D2699/D2700 (excepting PRF88.4)

[b] Anti-Knock Index (AKI) = (RON+MON)/2; Sensitivity (S) = RON-MON

[c] Measured in this work by ASTM D86 [36]

2.1.2. Gasoline surrogate fuels and their formulation

Four surrogate fuels were used in this work: one binary (PRF88.4) and three multi-component surrogates (PACE-1, PACE-8, and PACE-20). The primary reference fuel (PRF) was formulated using the anti-knock index (AKI) of RD5-87, as shown in Table 2. An attractive feature of PRF is that matching a known octane rating (RON, MON, or AKI) requires no expert knowledge or specialized tools. However, relative to a complex gasoline like RD5-87, PRFs lack octane sensitivity and have no aromatic or ethanol content among other shortcomings. Blends of TRF fuels and ethanol are not considered in this study, as their performance will most likely fall in between PRFs and multi-component fuels. To create higher fidelity surrogates, a working group of the PACE consortium [22] formulated three multi-component surrogates, in iterative fashion, targeting additional physical and chemical properties of RD5-87 as briefly outlined in the following discussion. It should be noted that the scope of this work does not include proposing and validating surrogate formulation methods.

PACE-1 is the initial surrogate fuel formulation proposed for use across a broad range of experimental and simulation studies. Table 1 provides the composition of the seven component PACE-1 surrogate fuel, which was generated via an optimization code, starting from an initial palette of components and set of fuel property targets. The method roughly follows those described in the review of Sarathy et al. [2] on common surrogate fuel formulation approaches, targets, and the significance of such targets. The initial palette of nine components listed in Table 1 was selected based on cost, purity, physical properties, and the availability and reliability of a component sub-model in the Lawrence Livermore National Laboratory (LLNL) detailed kinetic model. The following properties of RD5-87 were targeted: RON, MON, hydrogen to carbon ratio (H:C), liquid density, particulate matter index (PMI), hydrocarbon classes (PIONA), distillation curve temperatures, carbon numbers, and carbon types. A summary of the property estimation techniques will be given here. RON and MON were estimated separately using two independent feed-forward neural networks (FFNN) as described previously [37, 38]. H:C, carbon numbers, and carbon types were estimated from linear combinations of the mole fraction weighted component values. Carbon types were assigned using the classifications of Sarathy et al. [39]. Liquid density and hydrocarbon classes were estimated using linear combinations of the liquid fraction weighted component values, assuming perfect mixing behavior. Distillation curve temperatures were estimated via REFPROP [40]. Antoine parameters of neat components were used to estimate vapor pressures required to evaluate PMI [41] of the surrogate fuel. Liquid density and Antoine parameters for neat components were obtained from Yaws' Handbooks [42, 43].

PACE-1 was the first surrogate formulated and tested as part of this effort. As shown in Table 2, the measured RON and MON of PACE-1 are within 0.5 and 2.3 octane units of the RD5-87 target values and all other targeted values are captured well, with the notable exception of final boiling point. PACE-8 is a refinement of PACE-1 intended to more closely match the MON of RD5-87 while maintaining agreement with the other targeted properties. A Gaussian process regression (GPR) model mapping fuel composition to RON and MON was developed using literature measurements and new measurements made as part of this work. The GPR model was used in conjunction with the FFNN estimator to create multiple surrogates with estimated MON bracketing the desired MON. The proposed surrogate fuels were initially evaluated via standard tests such as ASTM D2699 for RON and ASTM D2700 for MON. The best matching one is termed as PACE-8 with measured RON and MON within 0.1 and 0.2 octane units of the RD5-87 target values. It is worth noting that the recommended ASTM reproducibility values of RON and MON are 0.7 and 0.9, respectively, for these measurements [4, 5]. Additional extensive testing of the surrogate fuels [22], including the present work, was also conducted.

PACE-20 represents the third iteration of design that improves the surrogate fuel fidelity in two key targets: the autoignition reactivity of RD5-87 at lean, HCCI-like conditions, and the high temperature distillation behavior. Autoignition reactivity was measured in the Sandia HCCI/LTGC research engine and simulated using an internal combustion engine reactor model in CHEMKIN. The computational expense of this model precluded use of an automated search and so relied on expert knowledge to manually adjust the formulation. Heat losses and in-cylinder minor species from residuals and EGR (such as CO and NOx) are included in the simulations. Two different numerical studies are performed: (a) an intake temperature sweep at $\phi_m = 0.40$ and naturally aspirated conditions, and (b) an intake pressure sweep at $\phi_m = 0.38$, where ϕ_m is the charge-mass equivalence ratio, which is defined in Section 2.3. Measurements of autoignition reactivity of RD5-87 and the four surrogate fuels in the ANL rapid compression machine and SNL HCCI/LTGC research engine are discussed in the Results and Discussion sections. To replicate the low volatility distillate of RD5-87, tetralin was used as an additional palette component. Tetralin exhibits a boiling point (208°C) and octane ratings (RON = 96.4, MON = 81.9) that are reasonably close to final boiling point and octane ratings of RD5-87, respectively (c.f. Table 2). RON and MON blending studies of tetralin in surrogate fuels, detailed in the Supplementary Material, confirm that small volumes can be added with minimal influence on octane ratings. Also, some 1,2,4-trimethylbenzene was swapped by toluene in formulating PACE-20. This was aiming to provide another degree of freedom to match all targeted properties without impacting other components or the overall concentration of aromatics.

The following minor differences in the property targets and estimation methods for PACE-20 relative to PACE-1 and PACE-8 are also given for completeness. RON and MON were estimated using the methods of Westbrook et al. [44] using offset corrections from the FFNN predictor. The measured RON and MON of PACE-20 (Table 2) are within 0.2 and 0.1 octane units of the RD5-87 target values, respectively, which are well within the recommended ASTM reproducibility values.

For PMI calculations, the approach of Burke et al. [45] was adopted to calculate the vapor pressures of components. Finally, additional properties of molecular weight (MW), lower heating value (LHV), and the stoichiometric air to fuel ratio (A/F_{stoich}) were targeted via linear blending models, while carbon types were not directly targeted during the formulation of PACE-20.

2.2. LTGC engine

2.2.1. Description

The Low-Temperature Gasoline Combustion (LTGC) research engine at Sandia National Laboratories (SNL) is used in this work [46]. This engine was derived from a Cummins B-series six-cylinder diesel engine and has been modified to work as a single-cylinder LTGC engine by deactivating cylinders 1 to 5. This facility has been widely used and validated in previous investigations, such as [47, 48]. Therefore, only a brief summary of the engine characteristics is presented here, while a more detailed description of the experimental facility and the experimental methodology can be found in [47-49].

The main characteristics of the engine are listed in Table 3. The toroidal-shaped piston bowl commonly used in diesel engines has been replaced by a custom piston that provides an open combustion chamber with a large squish clearance and small top ring-land crevice to minimize the unburned gases under LTGC operation. The geometric compression ratio is 16:1. Engine speed is controlled by a motor dynamometer that absorbs the power generated by the engine under combusting conditions and provides the power required to spin the engine under motoring (i.e., no combusting) conditions. Crankshaft position is measured with an incremental encoder with a resolution of 0.25 crank angle degrees. Physical TDC was verified experimentally to ensure a proper alignment of the shaft encoder. Premixed fueling is used in this investigation. The premixed fueling system is composed of a GDI injector that sprays into an electrically heated fuel-vaporizing chamber, which is connected to the intake pipe upstream of the intake plenum in a manner that ensures the mixing of the vapor fuel with the air and the EGR (if used) before the intake plenum. The whole intake system is preheated to a temperature close to the target engine intake temperature and at least to 60°C (333 K) to avoid condensation of the pre-vaporized fuel. An auxiliary electrical heater located close to the engine accurately controls the intake temperature and provides additional heating as needed (see [48, 50] for details). The effective engine intake temperature is monitored with two thermocouples located downstream the auxiliary heater that measure the gas temperature at the centerline and 2 mm away from the inner pipe wall. The deviation between the gas centerline temperature and the near-wall gas temperature was below 7°C for the conditions explored in this study. A positive displacement fuel flow meter (Max Machinery P002) provides an accurate measurement of fuel supplied to the engine. Intake air is supplied by an air compressor and the moisture is removed using a dehumidifier, while the airflow is precisely metered by a sonic nozzle. The cooling water and lubricating oil temperatures are kept constant at 100°C (373 K) for all tests. Exhaust emissions are measured using standard exhaust-gas analysis equipment by California Analytical Instruments, to obtain the CO, CO_2, unburned hydrocarbons (HC), nitrogen oxides (NO_x) and O_2 concentrations. In addition, a second CO_2 meter monitors the intake gases just prior to induction into the engine. This way, the composition of residuals and EGR can be estimated by solving mass and element balances.

Table 3. Key engine parameters and operating conditions.

SNL LTGC engine specification	
Displacement (single-cylinder) [L]	0.981
Bore [m]	0.102
Stroke [m]	0.120
Connecting rod length [m]	0.192
Geometric compression ratio	16:1
Effective compression ratio	15:1
No. of valves	4
Intake valve open [CAD]	0
Intake valve closure [CAD]	202
Exhaust valve open [CAD]	482
Exhaust valve closure [CAD]	8
Swirl ratio	0.9
Coolant/Oil temperature [K]	373
Engine speed [rpm]	1200

2.2.2. Experimental procedure

During all engine experiments, the engine speed, charge-mass equivalence ratio (ϕ_m), and ringing intensity (RI) are fixed at 1200 rpm, 0.38 and 5 MW/m^2, respectively. At naturally aspirated conditions, the whole intake system is pre-heated to 100°C and the engine intake temperature (T_{in}) is adjusted with an auxiliary intake heater for different fuels to maintain the target RI. At boosted conditions, T_{in} is set at 60 °C, which is the minimum intake temperature required to avoid fuel condensation in the intake system, and cooled EGR is used to maintain RI at 5 MW/m^2, since the CO_2 better absorbs the chemical heat release, and this suppresses gas dynamic development. The post-cooler EGR temperature is controlled by the engine operator and set to approximately 50°C.

In this work, the correlation for RI developed in [51] is used, which is treated as a measure of the propensity for engine knock. A criterion of RI = 5 MW/m^2 is selected since this value is the ringing limit for operation without knock in the LTGC engine, as used in previous works [47-49], which corresponds to about 8 bar/°CA at 1200 rpm, naturally aspirated. A complete discussion of the analysis and selection of this value can be found in [52].

Charge-mass equivalence ratio is defined based on the total charge mass as follows:

$$\phi_m = \frac{F/C}{(F/A)_{stoich}} \tag{1}$$

where F/C is the mass ratio between fuel and charge (air + EGR), and $(F/A)_{stoich}$ is the fuel-to-air mass ratio under stoichiometric conditions. This provides a convenient and consistent way to compare data with the same supplied energy content per unit charge mass, independently of the EGR rate or fuel used. It should be noted that ϕ_m is equal to the oxygen-based equivalence ratio, ϕ, if no EGR is used.

2.2.3. Data analysis

The cylinder pressure is measured by a water-cooled AVL QC34C pressure sensor flush-mounted in the cylinder head 42 mm off center. The data acquisition frequency is fixed at 0.25 CAD (28.8 kHz). The intake runner pressure is measured using a Taber model 2911, 0-100 psia, strain-gauge type pressure sensor. The in-cylinder pressure signal is pegged to the intake pressure near bottom dead center (BDC) where the cylinder pressure reading is virtually constant for several crank angle degrees. A 2.5 kHz low-pass filter [53] is applied to the in-cylinder pressure signal and 100 consecutive cycles are recorded and averaged to obtain a representative in-cylinder pressure trace. Top dead center (TDC) intake is defined as 0 CAD, so that TDC compression is at 360 CAD. The apparent heat release rate (AHRR) is computed from the in-cylinder pressure trace using standard slider/crank analysis [54], and it is corrected for heat transfer losses using the Woschni correlation [55]. The characteristic constants required for the heat transfer correlation are fitted for each combustion condition so that the HRR is null before and after the combustion process. The temperature evolution and the evolution of the mixture from reactants to products (based on the burn fraction) are used to compute the ratio of heat capacities (γ) in a piecewise manner. The 100-cycle averaged pressure signal is used for the HRR calculation, and the HRR is filtered with a piecewise smoothing function, as described in [48]. For tests with EGR, the EGR fraction is computed from the ratio of the intake and exhaust CO_2 concentrations. Uncertainty associated with this engine and the respective data analysis has been documented in [56].

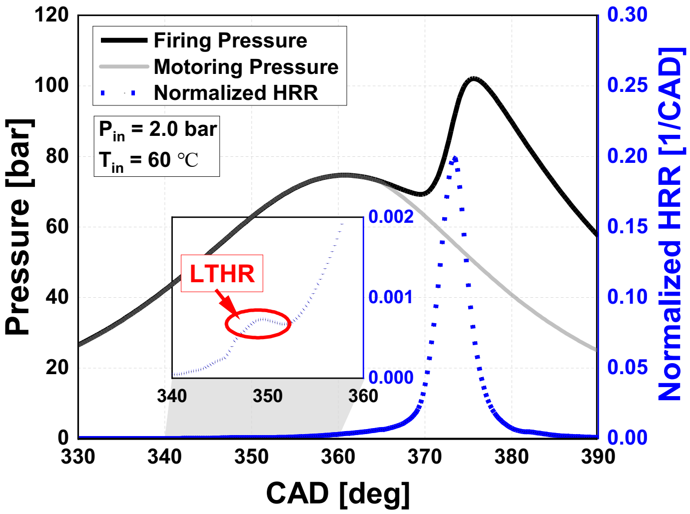

Figure 1. In-cylinder pressure and normalized heat release rate for RD5-87 at ϕ_m = 0.38, 1200 rpm, Pin = 2.0 bar, and Tin = 60 °C, with 53.5% exhaust gas recirculation used to maintain RI at 5 MW/m^2. Inset identifies LTHR.

The averaged in-cylinder pressure trace along with the corresponding calculated HRR normalized by total heat release (as opposed to the lower heating value of the charge) are presented in Fig. 1 for RD5-87 at Pin = 2.0 bar, and Tin = 60 °C. Lower heating value of the charge is not used for normalization as it requires accurate knowledge of the in-cylinder charge mass, which is challenging to determine for engines. In order to maintain a constant ϕ_m and RI at 0.38 and 5 MW/m^2, respectively, 53.5% EGR by mass is used. The inset elucidates the evolution of low temperature exothermicity. LTHR occurs at ~15 °bTDC (i.e., 345 CAD), and maintains for approximately 10 CAD, up to the second inflection point. ITHR takes place thereafter, and main ignition is reached at about 10 °aTDC.

2.3. Rapid compression machine

2.3.1. Description

A heated, twin-piston RCM (tpRCM) at Argonne National Laboratory (ANL) is utilized for this study. A detailed description of the configuration as well as uncertainties associated with experimental measurements can be found in [12, 13, 57], and is briefly provided here. The piston compression event is driven by the pneumatic system, and a hydraulic pin-groove arrangement is used to arrest the fast-moving pistons, allowing them to be hydraulically locked at the end of compression. The time for compression (t_{comp}) and last 50% of pressure rise (t_{50}), are approximately 15–18 ms and 1.9–2.0 ms, respectively, with higher compressed pressure (P_C) leading to slightly longer t_{comp} and t_{50}.

The reaction chamber and the two compression cylinders have an inner diameter of 50.8 mm, with a clearance height of nominally 25.5 mm at the end of compression. The stroke for each reaction chamber piston is 155.8 mm such that the geometric compression ratio (CR) is constant at 12.1:1, while compression heat loss results in an effective compression ratio ranging from 11.2:1 to 11.8:1, depending on the compressed state conditions, primarily Pc, and inert diluent conditions that affect the specific heat ratio of test mixture. The pistons utilize crevices machined around their circumference [57] to suppress possible vortex roll-up during the compression, thus improving post-compression charge homogeneity. The dynamic pressure in the reaction chamber is measured using a flush-mounted Kistler 6045A-U20 pressure transducer calibrated to 250 bar, and coupled to a Kistler Type 5064 charge amplifier. The transducer has a reinforced diaphragm for applications at excessive pressure rise rates. The thermal shock error of the transducer is estimated at $\Delta P_{max} < \pm 1\%$, and is used uncoated.

To accurately capture two-stage exothermic characteristics, the pressure signal can be split and recorded using two different National Instruments (NI) data acquisition cards. Since the first-stage heat release features much lower heat release rates, a 24-bit card is used for this study (NI 9239), sampled at 50 kHz. Higher rates of heat release, e.g., through the high temperature heat release (HTHR) process, are more robustly captured with a 16-bit card (NI 9223) sampled at 1 MHz. Goldsborough et al. [14] identified data acquisition and post-processing issues associated with heat release rate calculations. The pressure signal is filtered using the Savitzky-Golay algorithm with a second-order polynomial fit over a window of 0.2 ms (i.e., 11-point window for the 50 kHz data).

2.3.2. Mixture preparation

Mixtures of fuel, diluents (Ar, N_2 and CO_2), and O_2 are prepared in a 5.6 L, stainless steel tank, which is electrically heated to ~77 °C, and initially purged with inert gas and evacuated to < 0.1 mbar using an Edwards nXDS6i vacuum pump. A pre-determined mass of the liquid surrogate blend is first introduced into the tank through a septum, and then high-purity gases are supplied into the tank in the sequence of Ar (99.9997%, Airgas), N_2 (99.9998%, Airgas), CO_2 (99.9998%, Airgas) and O_2 (99.9997%, Airgas).

The manual filling valves placed upstream of the mixing tank inlet allow gases to be metered to within ±3 mbar of the desired value. Each feed requires an interval waiting time of 3–5 minutes to equilibrate the pressure of the tank, which is monitored using an MKS Baratron 628F (0–6666 mbar) heated manometer with a manufacturer specified uncertainty of ±0.25% of reading. After completion of each test batch, the mixture in the tank is isolated for at least 45 minutes to diffusively mix. Variations in the wait time have been explored, up to 3 h, with no noticeable change observed in measured ignition delay times. The evaporation efficiency of the liquid fuel is calculated based on ideal gas relations and is >95%, while the molar composition of the mixture is estimated from the partial pressure of gaseous components and the mass of fuel injected.

A fixed lean/undiluted fuel loading (21% O_2, ϕ =0.4) is studied in this work, in accordance with the LTGC engine experiments. Two diluent mixtures are adopted to cover low- to intermediate-temperature regimes. The test conditions used in this study are summarized in Table 4. Detail mole composition of the mixture, initial temperature and pressure for each test can be found in the Supplementary Material.

Table 4. Summary of test conditions used in the RCM.

Mixture #	**ϕ**	**O_2**	**N_2**	**Ar**	**CO_2**	**Tc**
Mix 1	0.4	~0.21	~0.66	0.00	~0.12	< 800 K
Mix 2	0.4	~0.21	~0.47	~0.31	0.00	> 800 K

* Gases are presented in mole percent.

2.3.3. Experimental procedure

The external surfaces of the reaction chamber and cylinders are heated to the desired temperature using electrical heating tapes with high-density insulation fitted between the flanges of the cylinders and the hydraulic chambers. The temperature on the outside surfaces of the reaction chamber and cylinders is periodically monitored using K-type thermocouples placed at 16 different positions along the cylinder and chamber surfaces. Thermal uniformity of ±0.2% is achieved in the axial and azimuthal directions across the exterior surface with at least 45 min of wait time. Initial reaction chamber temperatures from 30 to 85 °C are used to achieve desired range of compressed temperatures. It should be noted that the low initial temperature conditions in the reaction chamber (e.g., 30 °C in the reaction chamber vs. 77 °C in the mixing tank) will not cause fuel condensation since the fuel partial pressure in the reaction chamber is much lower (e.g., about 1/10) than those in the mixing tank and feeding line. More details of the temperature control of the reaction chamber can be found in [57]. The reaction chamber is then evacuated and purged several times using dry, bottled air (99.998% purify Airgas) before each filling event. The reaction chamber pressure is monitored using a second MKS Baratron 628F (0–6666 mbar) heated manometer. The test mixture is supplied into the reaction chamber to the targeted initial pressure using an MKS 248A-11094 electronic flow control valve through Polytetrafluoroethylene (PTFE)-lined and stainless-steel tubing heated to approximately 70 °C, which is controlled separately from the reaction chamber heating system. A proportional-integral-derivative (PID) controller is implemented in the LabVIEW control system to automate the filling procedure and control the reaction chamber pressure to within 0.15% of the desired value. After each filling event, the test mixture is allowed to equilibrate for at least 5 minutes in the chamber before commencing the test. A minimum of two shots are conducted at each compressed state to ensure repeatability. For these tests, repeatability is evaluated based on a number of factors, including compression time, time needed for the last 50% of pressure rise, the compressed thermodynamic condition (T and P), the first-stage and main ignition delay times, and pressure rise rates and peak pressure at main ignition. The high level of consistency of the tpRCM is demonstrated in Fig. S3 in the Supplementary Material via sixteen consecutive shots for ethanol/air mixture at Tc = 862 K and Pc = 20 bar.

2.3.4. Data analysis

The compressed temperature (Tc), ignition delay times and heat release rates are determined by post-processing recorded pressure traces. To ascertain the end of compression (t_0) and the extent of the heat loss during ignition delay period, a non-reactive test, wherein O_2 in the test mixture is replaced with N_2, is conducted for each reactive case.

The compressed temperatures are calculated using the adiabatic core hypothesis,

$$\int_{T_i}^{T_c} \frac{\gamma}{\gamma-1}\frac{dT}{T} = ln\frac{P_c}{P_i} \tag{2}$$

where the subscripts 'i' and 'c' indicate initial and compressed conditions, while γ is the ratio of specific heat of the gas mixture. The ideal gas law is applied over all the experimental conditions including pre- and post-compression, and the specific heat of the gas is taken to be a function of the mixture composition (determined based on equilibrium calculation) as well as the individual specific heat of the gas constituents. The specific heat of each gas constituent is estimated from polynomial fits of published data and as a function of temperature.

An energy balance approach [54] is used to calculate the heat release rates (HRR), and accumulated, or integrated heat release. The volumetric compression, and the accompanying heat loss and crevice flow processes are also incorporated into the analysis with the measured non-reacting pressure traces. Details of derivation of the heat release analysis have already been well-documented in [14], hence will not be repeated herein. The calculated HRR can be expressed as,

$$HRR = \frac{\gamma}{\gamma - 1}\frac{dV}{dt}[P - P_{nr}] + \frac{1}{\gamma - 1}V\left[\frac{dP}{dt} - \left.\frac{dP}{dt}\right|_{nr}\right] - \frac{PV}{(\gamma - 1)^2}\left[\frac{d\gamma}{dt} - \left.\frac{d\gamma}{dt}\right|_{nr}\right] \tag{3}$$

where the subscript $'nr'$ indicates non-reacting condition. The gas temperature during the reactive tests is calculated using ideal gas law, i.e., $\left(\frac{P}{P_{nr}}\right) = \frac{T}{T_{nr}} \cdot \frac{MW_{nr}}{MW}$, where MW is the mean molecular weight determined based on mixture composition. It should be noted that the calculation of gas temperature for the reactive case differs from that used in [14].

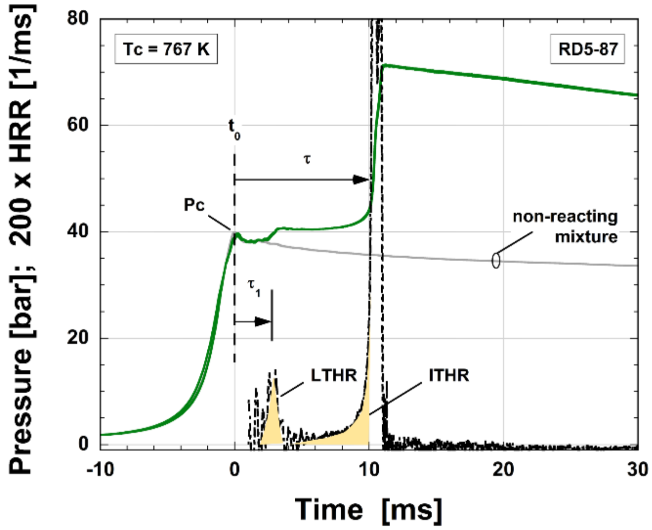

Figure 2. Measured, representative reactive and non-reactive pressure-time histories and calculated heat release rate at Pc = 40 bar, Tc = 767 K for RD5-87, with τ_1, τ, LTHR and ITHR identified. HRR is normalized by $\mathrm{LHV_{mix}}$. PACE-20 composition is used for HRR calculation for RD5-87.

Figure 2 presents two representative reactive traces along with the associated non-reactive trace for RD5-87, where consistency between the two reactive shots, and alignment between the non-reactive and reactive traces prior to preliminary heat release events are excellent. The composition of PACE-20 is adopted for the calculation of HRR for RD5-87. A comparison between different surrogates (PACE-1, PACE-8 and PACE-20) in specific heat ratio can be found in Fig. S4 in the Supplementary Material, where the difference between different surrogates is found to be very small across the temperatures studied in this work. The impact from using different surrogates on the calculation of heat release rates is therefore negligible. Ignition delay times for first-stage (τ_1) and main ignition (τ) are also highlighted in Fig. 2, along with the LTHR (low temperature heat release) and ITHR (intermediate temperature heat release) inferred from the accumulated HRR. Note that all heat release calculations presented in this work are normalized by the LHV of the test mixture, e.g., (J/mol/ms)/(J/mol).

Uncertainty analyses associated with ANL's tpRCM were presented in [57, 58], using a linear propagation approach similar to [59]. The uncertainty in computed Tc is estimated at 1.0-1.5%, due to instrumentation imprecision and procedural uncertainties associated with mixture preparation, and an uncertainty of ±0.4 ms is estimated for each ignition delay measurement to account for the improper alignment with the non-reacting traces. Excellent consistency is achievable in the ANL tpRCM throughout the day, or week. Statistical (i.e., month-to-month) variability in τ however, can be on the order of ±10%. It is important to recognize that quantifying the impact of Tc's uncertainty on τ is not straightforward due to the probability distribution of Tc within its uncertainty, interplay between Tc and other parameters given highly non-linear relations between Tc and τ, etc. Established frameworks of uncertainty quantification, such as [60, 61], can be adopted for such evaluation in the future, but is beyond the scope of this study. The relative uncertainty in calculation of heat release due to measurement uncertainties is estimated at ±6–7%, as discussed in [14, 58]; this does not take into account systematic uncertainties associated with the calculation framework that employs the single-zone formulation and the application of adiabatic core hypothesis, which cannot account for exothermically-driven heat loss and gas transport to the piston crevice volumes, or growth of the boundary layer at very long τ.

3. Computational

The gasoline surrogate kinetic model developed in [12] is used in this study. It is based on the "core" C0–C4 sub-model developed by National University of Ireland, Galway (NUIG) [62], with reaction rate rules and thermochemistry extensively updated for typical PIONA components. Readers are encouraged to find more details in [12]. The ethanol sub-chemistry at low to intermediate temperatures has been updated following recent studies. Details regarding these, and associated validation against experiments can be found in [12, 63-66].

Simulations of the RCM experiments are completed using the LLNL-developed fast solver Zero-RK [67], with volume-time histories for the RCM experiments derived from non-reactive tests accounting for compression and heat loss [13]. The volume-time histories are derived following isentropic relations (i.e., $(\frac{V}{V_i})^{\gamma} = (\frac{P_i}{P})$, where P_i is the initial pressure in the reaction chamber, V_i is the initial reaction chamber volume, P is the measured pressure from the non-reactive case, V is the volume of the adiabatic core, and γ is the ratio of specific heat of the gas mixture assumed as functions of mixture composition and temperature).

4. RESULTS AND DISCUSSION

4.1. LTGC engine

RD5-87 and the three multi-component surrogate fuels (namely PACE-1, PACE-8 and PACE-20) are tested in the Sandia LTGC research engine under fully-premixed HCCI-like conditions at P_{in} = 1.0 bar (naturally aspirated conditions) and P_{in} = 2.0 bar (high-boost conditions). It should be noted that the P_{in} = 2.0 bar condition is defined as “high boost” to differentiate from the P_{in} = 1.3 bar condition (discussed in Fig. 5), rather than implying that this is the condition typically used in commercial compression ignition engines where the boosted intake air pressure can be much higher than 2 bar. The overall reactivity and exothermic behavior are evaluated for the four fuels. As discussed in Section 2.2.2, at naturally aspirated conditions, the intake temperature is adjusted to obtain a CA50 that gives RI = 5 WM/m^2, while at high-boost conditions, the EGR rate is adjusted to obtain a CA50 with RI = 5 WM/m^2. Therefore, at P_{in} = 1.0 bar, the intake temperature deviation between RD5-87 and the surrogates is a metric indicating the ability of the multi-component fuels to replicate the reactivity of RD5-87, while at P_{in} = 2.0 bar, the in-cylinder O_2 content is a metric of the reactivity of the fuels, where the in-cylinder O_2 deviation between RD5-87 and the surrogates quantifies the ability of the multi-component surrogates to replicate the reactivity of the full-boiling-range gasoline.

Figure 3 shows the in-cylinder pressure-temperature (P-T) trajectories for all the fuels at Pin = 1.0 and 2.0 bar. The P-T trajectories for the four fuels are slightly different from each other due to the different intake temperatures and EGR rates (where the EGR rate affects the compressed-gas temperature and pressure via changes to the specific heat ratio). The P-T trajectories of the RON and the MON tests for RD5-87 are also included for reference. It can be seen from Fig. 3 that LTGC experiments at Pin = 1.0 bar and 2.0 bar correspond to high-temperature/low-pressure "beyond MON" and low-temperature/high-pressure "beyond RON" conditions, respectively. As such, the LTGC experiments evaluate the reactivity of the fuels for both the high-temperature and the low-temperature autoignition regimes.

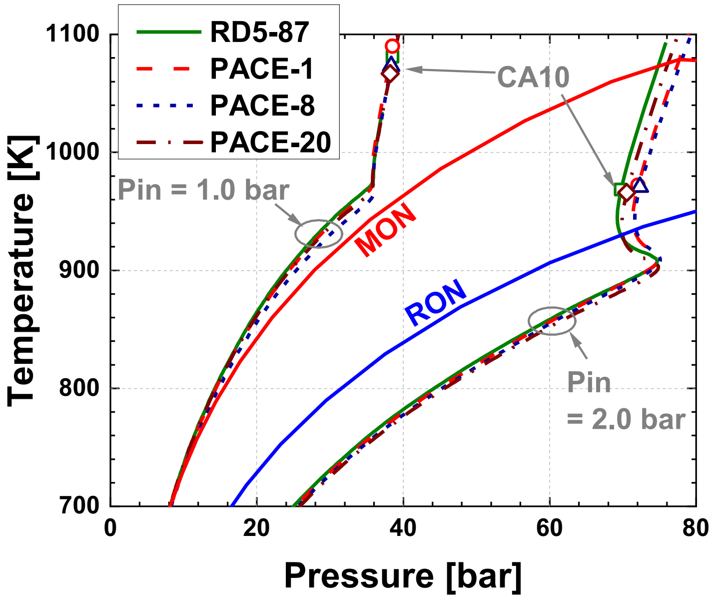

Figure 3. P-T trajectories at 1200 rpm, $\phi_m = 0.38$, RI = 5 WM/m^2, and $P_{in} = 1.0$ and 2.0 bar for RD5-87, PACE-1, PACE-8 and PACE-20. The trajectories of the RON (blue) and MON (red) tests for RD5-87 are also included in the figure. Symbols represent CA10 for the surrogates. T_{in} at $P_{in} = 1.0$ bar and in-cylinder O_2 at $P_{in} = 2.0$ bar for different fuels are summarized in Table 5.

Table 5 summarizes the intake temperature (for P_{in} = 1.0 bar data) and in-cylinder O_2 content (for Pin = 2.0 bar) of the experiments with RD5-87 and the surrogate fuels. As can be seen, for P_{in} = 1.0 bar, the intake temperatures required by PACE-1 and PACE-8 are 5.5°C and 5.7°C lower than that of RD5-87, respectively, which correspond to deviations of -4.6% and -4.8% in °C, respectively, meaning they are more reactive. On the other hand, the intake temperature required by PACE-20 is only 1.2°C lower than that of RD5-87, which corresponds to an intake temperature deviation of -1.0%. This value is within the repeatability of the engine facility and, therefore, beyond our capability to distinguish between fuels. For P_{in} = 2.0 bar, the in-cylinder O_2 content required by PACE-1 and PACE-8 is 1.17% and 0.84% lower than that of RD5-87, respectively, which correspond to deviations of -10.1% and -7.3%, respectively, relative to the in-cylinder O_2 content of RD5-87. The in-cylinder O_2 content required by PACE-20 is virtually identical to that of RD5-87, which again implies that PACE-20 properly replicates the change of RD5-87 reactivity with boosting.

Table 5. Intake temperature at P_{in} = 1.0 bar and in-cylinder O_2 at P_{in} = 2.0 bar required in the experiments

	P_{in} = 1.0 bar				**P_{in} = 2.0 bar**			
	T_{in} (°C)	**T_{in} deviation vs. RD5-87 (°C)**	**CA10**	**CA10-90**	**In-cyl. O_2 at**	**O_2 deviation vs. RD5-87**	**CA10**	**CA10-90**
RD5-87	119.2°C	-	364.8	3.8	11.60%	-	370.2	6.0
PACE-1	113.7°C	-5.5°C	365.4	3.9	10.43%	-1.17%	369.0	6.0
PACE-8	113.5°C	-5.7°C	365.4	3.9	10.76%	-0.84%	368.9	6.0
PACE-20	118.0°C	-1.2°C	365.1	3.9	11.59%	-0.01%	369.9	6.0

The exothermic behavior of the four fuels is described next. Figure 4 shows the normalized HRR of RD5-87 and the three multi-component surrogates at "beyond MON" (Fig. 4a) and "beyond RON" conditions (Fig. 4b). The HRR is plotted against the crank angle relative to the crank angle of the 50% burn point (i.e., CAD – CA50) for a better comparison between different fuels. Only the early part of the heat release curve covering the LTHR and ITHR processes are shown in the figure to allow higher resolution. Fig. 4a shows that at the "beyond MON" condition where LTHR is not observed, both PACE-1 and PACE-8 exhibit greater ITHR than RD5-87, while the ITHR of PACE-20 closely agrees with that of RD5-87. This corresponds with the trends in Table 5, where PACE-1 and PACE-8 are more reactive than RD5-87 at naturally aspirated conditions. The promoting effect of ITHR on autoignition reactivity is also consistent with previous studies [66, 68]. When P_{in} is increased to 2.0 bar, and the P-T trajectory is shifted into the "beyond RON" region (Fig. 3), LTHR is observed for all the fuels, as seen in Fig. 4b. Comparing to RD5-87, both PACE-1 and PACE-8 display stronger LTHR, while PACE-20 behaves similarly to RD5-87. The stronger LTHR for PACE-1 and PACE-8 corresponds with to their stronger autoignition reactivity as seen in Table 5 where LTHR can advance combustion phasing [13]. Despite the difference in LTHR, all the fuels show virtually the same ITHR at P_{in} = 2.0 bar.

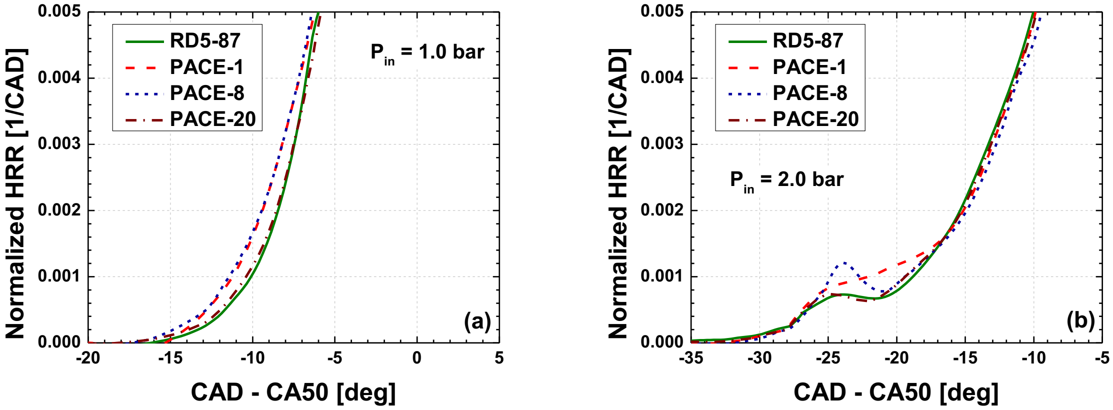

Figure 4. Normalized heat release rate as functions of crank angle relative to CA50 (i.e., CAD – CA50) for RD5-87 and the surrogates at (a) P_{in} = 1.0 bar and (b) P_{in} = 2.0 bar. Only the early part of the HRR covering LTHR and ITHR is shown in the figure. T_{in} at P_{in} = 1.0 bar and in-cylinder O_2 at P_{in} = 2.0 bar for different fuels are summarized in Table 5.

4.2. RCM

RD5-87 and the four surrogates are further tested in the ANL tpRCM at four compressed pressure conditions (i.e., Pc = 15, 25, 40 and 60 bar) covering compressed temperatures from 680 to 955 K. These conditions span the ‘preignition’ range traversed within the LTGC engine experiments, as seen in Fig. 3. To demonstrate the correlation between the tpRCM and the LTGC engine, isopleths of accumulated LTHR (presented in %LHV), first-stage and main ignition delay times of RD5-87 acquired from the tpRCM are shown in Fig. 5 in a P-T space, together with the RD5-87 P-T trajectories from the LGTC engine at three different intake pressures (i.e., Pin = 1.0, 1.3 and 2.0 bar). The changes in temperature sensitivity for the main ignition isopleths at Tc ~ 900 K indicate NTC behavior, which shifts to higher temperatures with increased compressed pressure. Around halfway through the NTC region (e.g., Tc ~ 800 K), two-stage ignition behavior exhibits with LTHR accompanying, which are characterized by the isopleths of accumulated LTHR and first-stage ignition delay times. By comparing the engine trajectories with the RCM datasets, it is clear that conditions experienced in the LGTC engine are directly mapped by the autoignition regimes quantified in the tpRCM, indicating the reliability to use the tpRCM data to infer fuel behavior under HCCI-like conditions in the LGTC engine. Specifically, taking the isopleth map as reference, it is obvious that the engine trajectory at P_{in} = 1.0 bar traverses through the intermediate-temperature regime with no LTHR, whereas at P_{in} = 2.0 bar, the engine trajectory shifts toward the low-temperature/high-pressure regime where LTHR occurs. These inferences based on RCM measurements corroborate well with the results in Fig. 4, where RD5-87 displays no LTHR at P_{in} = 1.0 bar, while exhibiting LTHR at P_{in} = 2.0 bar.

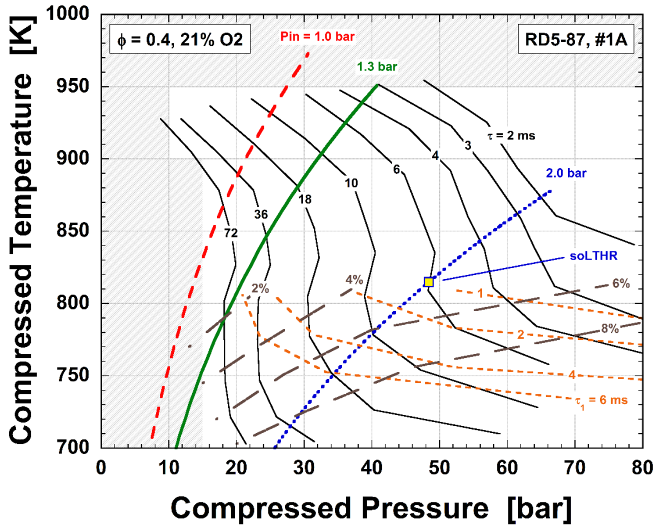

Figure 5. LTGC engine P-T trajectories overlaid on isopleths of τ = 2–72 ms for RD5-87. Isopleth for first-stage ignition (dashed orange lines) and accumulated LTHR (black dashed lines, present as percent of total energy) are also shown. P-T trajectories from LTGC engine are shown for P_{in} = 1.0, 1.3 and 2.0 bar that correspond to naturally aspirated, boost and high-boost engine operation, respectively.

Figure 6 next illustrates the representative pressure-time histories at Pc = 40 bar and two compressed temperatures, i.e., Tc = 760 and 900 K, within the low-temperature/NTC and intermediate temperature regimes, respectively, along with the corresponding non-reactive pressure-time history. It should be noted that at least two tests were conducted at each condition, with great consistency observed.

At Tc = 760 K (Fig. 6a), RD5-87 exhibits two-stage ignition behavior. This is qualitatively replicated by all four surrogates, though quantitative differences in their reactivity are observed. Compared to RD5-87, PACE-1, PACE-8 and PRF88.4 are more reactive achieving main ignition, while PACE-1 and PACE-8 display similar first-stage ignition reactivity. PACE-20 nearly overlays with the RD5-87 pressure-time history, replicating the first-stage and main ignition reactivity, as well as the inflection point in pressure rise during main ignition. Also seen in Fig. 6a is the different compression trajectory for PACE-1 as compared to others. This is caused by the asynchronicity of the two pistons, which do not affect the results in the present study since the chemical reactivity prior to end of compression at this condition is negligible, as can be inferred from the alignment at end of compression between the reactive and non-reactive tests. At Tc = 900 K (Fig. 6b), single-stage ignition behavior is present for RD5-87 and all surrogates. Similar to the quantitative trends observed at Tc = 760 K, all surrogates tend to be more reactive than RD5-87 at Tc = 900 K, with PACE-20 showing the closest agreement with RD5-87. Simulated pressure-time histories are also shown in the lower panels in Fig. 6. Although the model captures the two-stage and single-stage ignition behaviors at Tc = 760 and 900 K, respectively, for all surrogates, it consistently underpredicts the reactivity for PACE-1, PACE-8 and PRF88.4 at both temperatures, with greater discrepancies obtained at Tc = 750 K. Nevertheless, it is worth noting that excellent agreement in main ignition reactivity is observed for PACE-20, which was the surrogate down-selected for the PACE project.

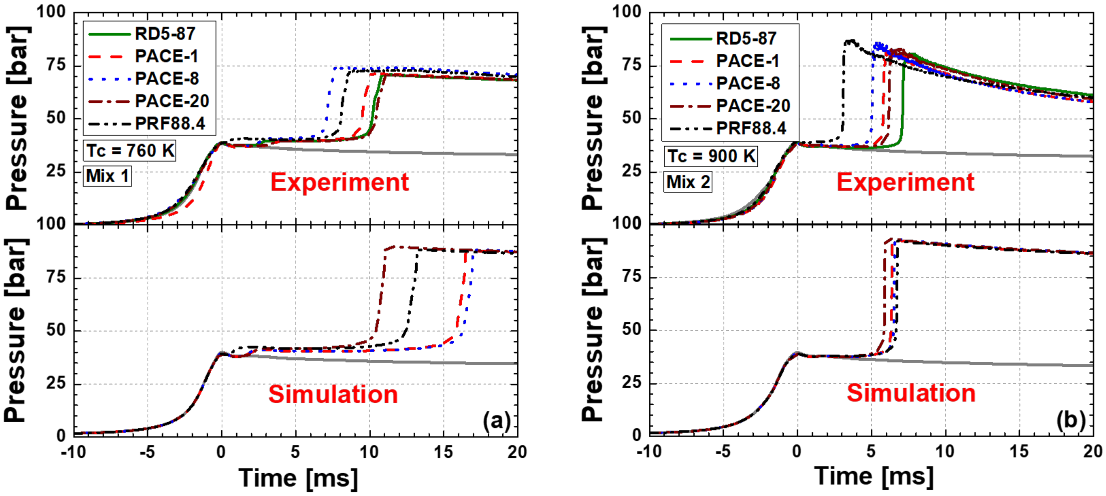

Figure 6. Measured and simulated pressure-time histories for RD5-87 and it surrogates at ϕ = 0.4, 21% O_2, Pc = 40 bar, and (a) Tc = 760 K and (b) 900 K, with corresponding non-reactive results also included. Upper panels are experiments, and lower panels are model results.

To better evaluate the surrogate performance in replicating RD5-87 autoignition characteristics, first-stage and main ignition delay times for each surrogate are compared to those of RD5-87 in Fig. 7 across wider temperature ranges for the four pressure conditions studied. Here, it can be seen from Fig. 7 that all surrogates are able to reproduce the global trends of RD5-87, including the typical low-temperature/NTC behaviors, and Arrhenius behavior at intermediate temperatures, with similar qualitative pressure effects on both first-stage and main ignition reactivity. It is important to recognize that compressed conditions in the reactive tests will differ greatly from the non-reactive tests if compression reactivity is significant. The compressed pressures in the reactive tests in this study are quite close to the respective non-reactive tests, as can be seen in the Supplementary Material, indicating that compression reactivity for the dataset presented in Fig. 7 is insignificant.

Figure 7a indicates that PACE-1 is overall more reactive than RD5-87, with better agreement observed at low and intermediate temperatures, and greater discrepancies observed at NTC temperatures (particularly the intersecting temperatures from NTC regime to intermediate-temperature regime at about 850 K). As pressure increases, the discrepancy at low temperatures diminishes, while that at high temperature becomes more obvious. Despite these discrepancies in main ignition reactivity, the level of agreement between PACE-1 and RD5-87 in first-stage ignition reactivity is good, as can be seen in Fig. 7b.

PACE-8 (Figs. 7c and 7d) performs similarly to PACE-1, displaying greater main ignition reactivity with similar first-stage ignition reactivity in comparison to RD5-87. At lower temperatures and pressures (e.g., Tc < 800 K and Pc = 15 bar), PACE-8 is less adequate than PACE-1 in capturing RD5-87 main ignition reactivity, exhibiting much shorter main ignition delay than

RD5-87. The disagreement at low temperatures and pressures, however, quickly diminishes at Pc > 40 bar, leading to similar performance between PACE-1 and PACE-8. At higher temperatures (i.e., Tc > 830 K), with a better match in MON compared to PACE-1 (as shown in Table 2 and discussed in Section 2.1.2), PACE-8 reproduces better than PACE-1 the ignition delay times at low pressures (e.g., Pc = 15 bar). However, this agreement deteriorates rapidly as pressure is increased above 25 bar. At the highest pressure studied (i.e., Pc = 60 bar), the better match in MON for PACE-8 than for PACE-1 does not lead to better agreement in intermediate/high temperature reactivity with RD5-87.

PACE-20 (Figs. 7e and 7f), with lean, HCCI-like autoignition reactivity used as additional targets for surrogate formulation, is seen to better capture both first-stage and main ignition delay times at all pressures and temperatures studied. The refinement in the ratio of *n*- to *iso*-paraffin concentrations (as shown in Table 1) leads to reduced NTC strength at low pressures, but more pronounced NTC behavior at high pressures compared to PACE-1 and PACE-8, resulting in greatly improved agreement with RD5-87. The remarkable agreement at different compressed pressures indicates that PACE-20 can adequately replicate RD5-87 under different levels of intake boosting, which corroborates the LTGC engine results.

Finally, PRF88.4 (Figs. 7g and 7h) is seen to only capture RD5-87 behavior at low pressures of 15 – 25 bar, whereas it is considerably more reactive at Pc ≥ 40 bar. In addition, the binary surrogate is unable to replicate the first-stage ignition characteristics of RD5-87, where considerably faster first-stage ignition times are recorded for PRF88.4 than RD5-87, with the level of discrepancy becoming greater at higher temperatures. The large discrepancies at high-pressure conditions suggest that PRF88.4 should not be used to represent RD5-87 in boosted engines, and that targeting only AKI is not sufficient for surrogates to capture gasoline autoignition reactivity under HCCI-like conditions, as also seen in [14].

The model results in Fig. 7 are seen to capture well the experimental measurements of PACE-20 at all temperatures and pressures, whereas some discrepancies are observed for the other three surrogates. Specifically, the model underpredicts the main ignition reactivity for PACE-1, PACE-8 and PRF88.4, particularly at high-pressure conditions and NTC temperatures. The NTC behavior is also less pronounced in the simulations results than in the experiments, which is most obvious for PRF88.4. In contrast to the low-temperature measurements, ignition delay times at intermediate-temperatures are better captured by the model. Despite these discrepancies, the capability of the model to capture both the qualitative and quantitative trends of PACE-20 is encouraging. The model shows the largest disagreement with experiments for PRF88.4 among the four surrogates. This is somewhat counter-intuitive since PRF chemistries should have been validated the most in the past among all surrogate components. It should be noted that the model used in this study has been extensively validated against ignition and species experiments for n-heptane [69] and iso-octane [70] in the past, mostly at conditions around stoichiometry and pressures below 50 bar, but not at the lean/high-pressure conditions in this study (e.g., 60 bar and phi = 0.4), where model shows the largest disagreement with the experiments (c.f. Fig. 7g). The largest disagreement is observed at NTC temperatures. NTC behavior is related to the equilibrium of $R\cdot+O_2=RO\dot{O}$. This equilibrium is quite sensitive to pressure and O_2 concentration, which can be significantly affect by changes in pressure and fuel loading conditions, and are likely the major cause of the discrepancies observed in Fig. 7. Further investigations on this issue are recommended.

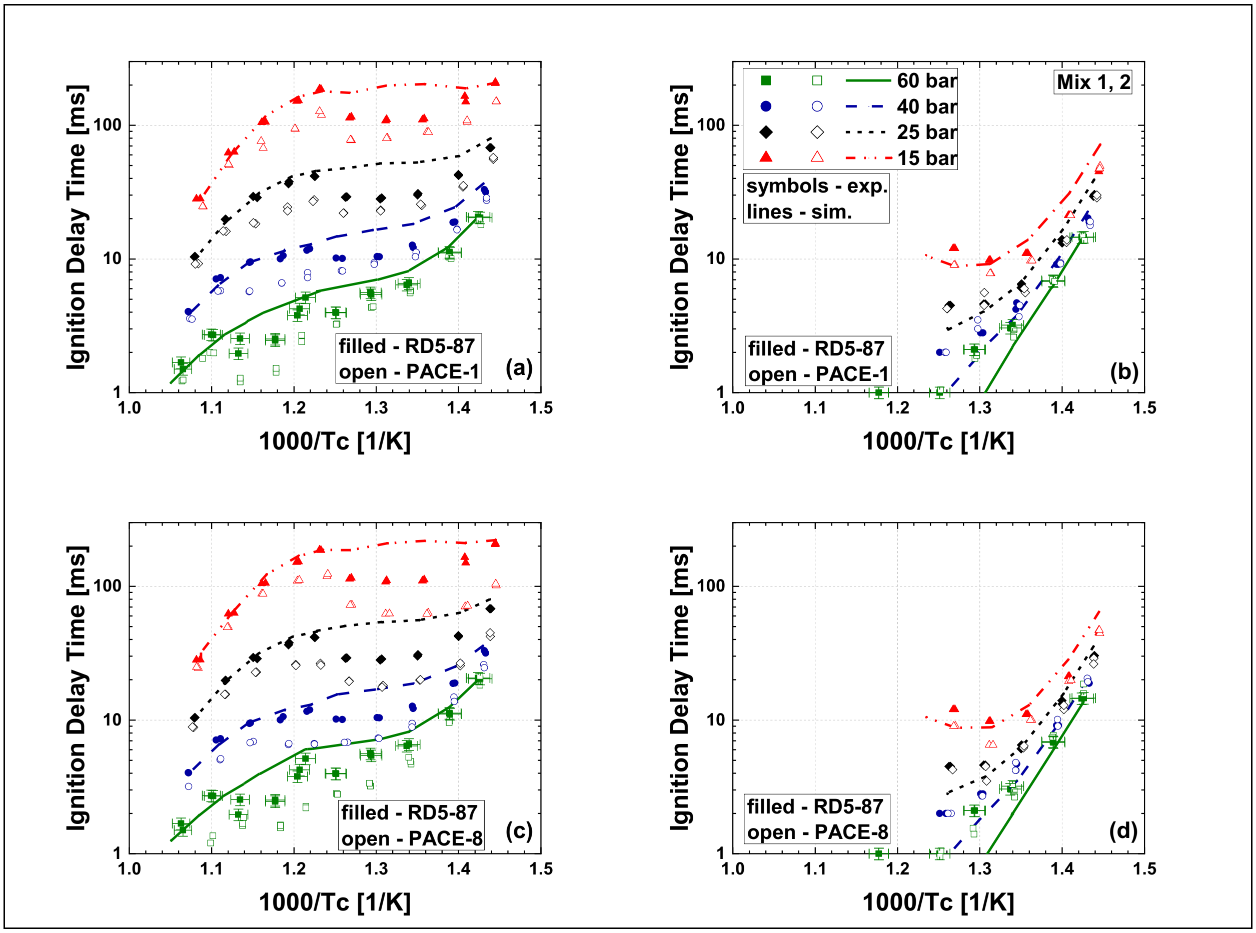
Ignition Delay Time [ms]
1000/Tc [1/K]
1
10
100
1.0
1.1
1.2
1.3
1.4
1.5
filled - RD5-87
open - PACE-1
(a)
60 bar
40 bar
25 bar
15 bar
Mix 1, 2
symbols - exp.
lines - sim.
filled - RD5-87
open - PACE-1
(b)
filled - RD5-87
open - PACE-8
(c)
filled - RD5-87
open - PACE-8
(d)

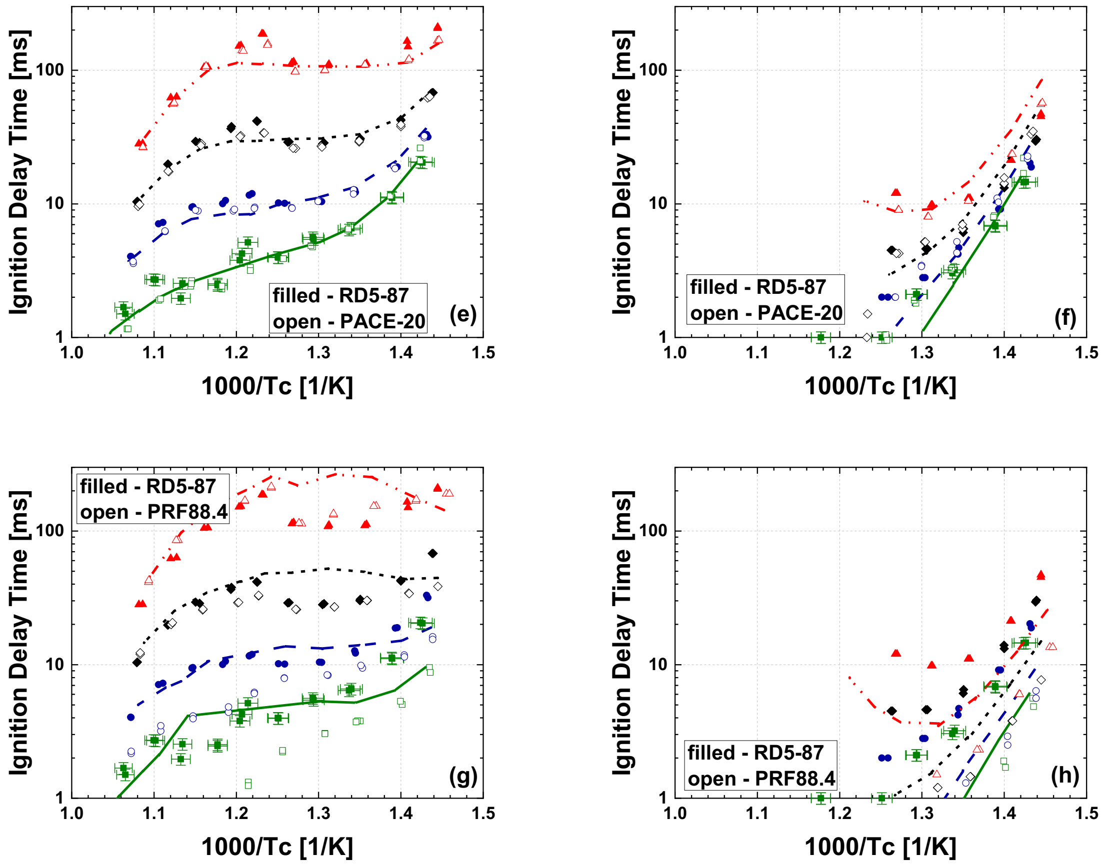

Figure 7. Comparison of measured and simulated first-stage (right panels) and main ignition delay times (left panels) between RD5-87 and (a)–(b) PACE-1, (c)–(d) PACE-8, (e)–(f) PACE-20 and (g)–(h) PRF88.4 at ϕ = 0.4 and 21% O_2. Lines are simulation results, and symbols are experiments.

Given the good alignment between the tpRCM and the LTGC engine, as seen in Fig. 5, isopleths for each surrogate are further compared with those for RD5-87 across the same P-T space as in Fig. 5, aiming to characterize the surrogate performance in a manner indicative of HCCI engine operation (i.e., under constant combustion phasing). The measured and simulated first-stage and main ignition isopleths are presented in Fig. 8. Within the low-boost/intermediate-temperature regime (e.g., Pc < 30 bar and Tc > 850 K), the four surrogates capture RD5-87 isopleths reasonably well, with PACE-20 outperforming PACE-1, PACE-8 and

PRF88.4. However, within the high-boost/low-temperature regime (Pc >40 bar and Tc < 800 K), which is more relevant to boosted/low-temperature compression ignition engines, PACE-1, PACE-8 and PRF88.4 isopleths deviate significantly from those of RD5-87, while PACE-20 isopleths nearly overlap with those of RD5-87. Under constant combustion phasing scenarios, it is obvious that PRF88.4 performs the worst in capturing RD5-87 phasing, particularly at short timescales representative of engine combustion (e.g., isopleths of main ignition below 4 ms). Comparing the measurements with the corresponding modeling results, it is evident that the model underpredicts the NTC behavior for all surrogates, with the worst agreement observed for PRF88.4.

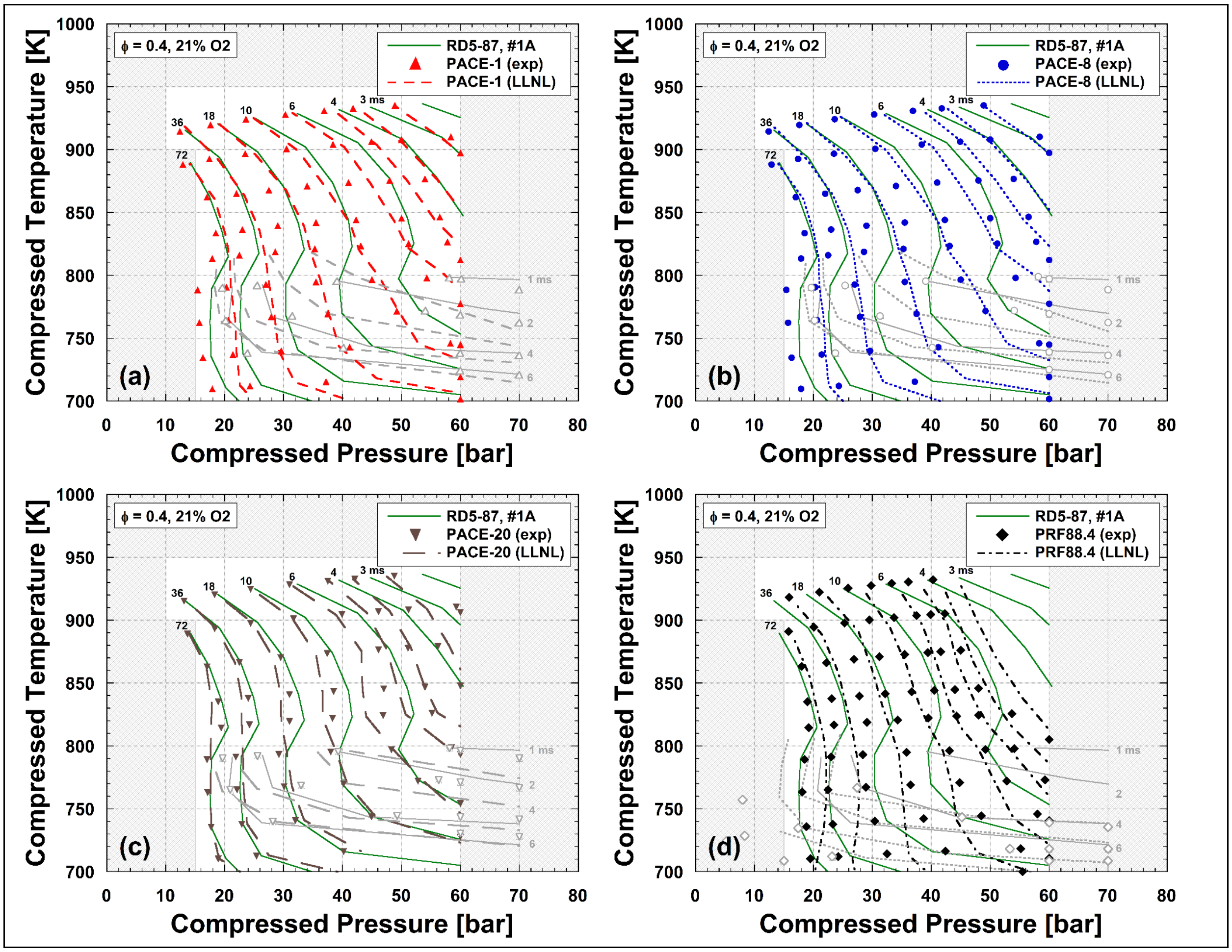

Figure 8. Comparison of isopleth of first-stage (gray symbols and lines) and main ignition delay time (color symbols and lines) between RD5-87 and (a) PACE-1, (b) PACE-8, (c) PACE-20 and (d) PRF88.4 at $\phi = 0.4$ and 21% O_2. Solid lines are experimental results for RD5-87; symbols are experimental ignition delay times for surrogates; non-solid lines are simulation results for the surrogates.

The ignition delay time results presented in Figs. 7 and 8 reveal the ability of the four surrogates in mimicking RD5-87 autoignition characteristics at lean/HCCI-like conditions, both with and without intake boosting, which follows the order of PACE-20 > PACE-1 > PACE-8 > PRF88.4. All surrogates are seemingly adequate under naturally aspirated conditions, since at this condition the P-T trajectory only traverses through the low-pressure/high-temperature regime (c.f. Fig. 5) where all surrogates replicate RD5-87 reasonably well (c.f. Fig. 8). However, the performance of PACE-1, PACE-8 and, particularly, PRF88.4 deteriorates rapidly at highly boosted conditions that are more relevant to boosted engine operation. It is evident from these comparisons that multi-component surrogates are superior to the binary surrogate (i.e., PRFs). Also, it is interesting that a better match in MON led to greater disagreement at high-pressure conditions that are more representative of boosted engine operation (see comparison between PACE-1 and PACE-8 in Fig. 7), indicating the insignificant contribution of MON toward improving surrogate fidelity when it is used as a target for HCCI-like conditions. On the other hand, the lean/HCCI-like autoignition characteristics that were used as additional targets for PACE-20 allow PACE-20 to adequately capture the autoignition characteristics of RD5-87 at the lean conditions investigated in this study, highlighting the necessity of including non-standardized fuel properties as additional validation targets for the formulation of high-fidelity gasoline surrogates.

To elucidate the surrogate performance in capturing the exothermic behavior during autoignition of RD5-87, LHV-normalized heat release rates from the RCM experiments are presented in Figs. 9 and 10 as functions of core gas temperature for the same conditions as in Fig. 6. At Tc = 760 K, immediately seen in Fig. 9a is the three-stage heat release behavior of RD5-87, where the first-, second- and third-stage heat release occur over the temperature ranges of 750–850, 850–1350 and 1350–1600 K, respectively. This behavior is reproduced by all four surrogates. Excellent agreement is obtained between PACE-20 and RD5-87, where the difference between their HRR trajectories is within typical levels of uncertainty in calculated heat release rate. PACE-8 is slightly inferior to PACE-20 in mimicking RD5-87 heat release characteristics, mainly due to the slightly extended heat release process in all three stages. PACE-1 and PRF88.4 exhibit much stronger LTHR, as well as higher magnitudes of intermediate- and high-temperature heat release than RD5-87. The model (Fig. 9b) replicates the multiple stages of heat release for all surrogates, though quantitative differences exist. For instance, LTHR characteristics are better predicted by the model for PACE-1 and PACE-8, and overpredicted by the model for PACE-20, and especially PRF88.4. Meanwhile, the last stage of heat release, where CO is converted to CO_2, is overpredicted by the model, both in terms of rate and magnitude of temperature increase achieved. Note that the experimental measurements indicate substantially lower peak temperature than the model results. This could be due to gas flow into the crevice, and/or quenching of HTHR in the reaction chamber, where the accumulated CO is not completely oxidized to CO_2. It could also be due to treating the RCM as a single computational zone in the simulations. Further investigation is needed to resolve these discrepancies.

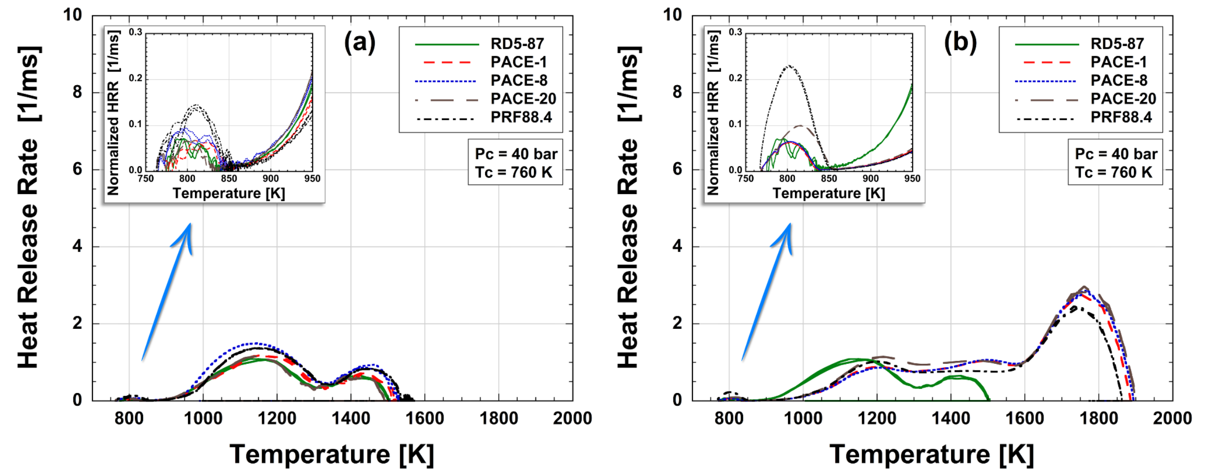

Figure 9. Heat release rate presented as functions of core gas temperature for RD5-867 and the four surrogates at ϕ = 0.4, 21% O_2, Pc = 40 bar and Tc = 760 K. (a) experimental results; (b) simulation results. The results for RD5-87 in both plots (solid green lines) are experimental results.

At Tc = 900 K (Fig. 10), as expected, LTHR is completed suppressed and single-stage heat release behavior is observed for RD5-87. This is again captured by all surrogates, with better agreement obtained for PACE-1 and PACE-20. The largest discrepancies are also expressed by PRF88.4, the bi-component surrogate. The model predicts similar heat release behavior for all the surrogates, which is consistent with the simulated pressure-time histories in Fig. 6b. Also evident is that the model predicts higher rates of heat release, leading to higher peak core gas temperatures. This is again due in part to assumptions made in the variable-volume simulations, where the volume-time histories derived from non-reactive tests do not account for exothermically-driven heat loss and gas transport to the piston crevices in the reactive experiments. Note that the ringing in the experimental HRR curves at the completion of heat release is due in part, to mechanical and electromagnetic noise in the pressure records. It should be noted that despite the similar qualitative trends between Fig. 4 and Figs 8 & 9, direct, quantitative comparison in HRR between the LTGC engine and the tpRCM is not made, due primarily to: (1) different normalization methods are used (total heat release for LTGC engine vs. LHV of the mixture for tpRCM); (2) the considerably different timescales between the two test facilities (i.e., 1 ms = 7.2 CAD).

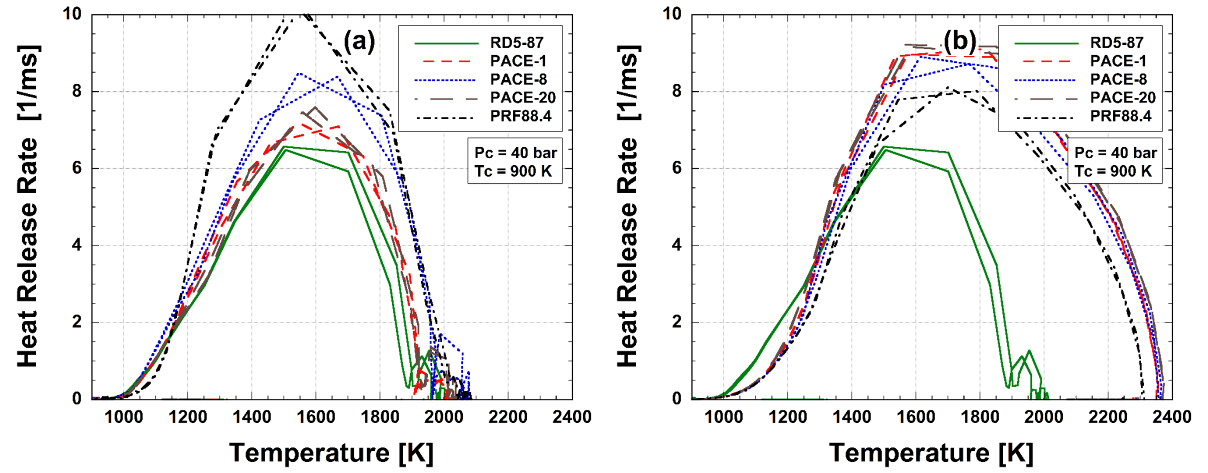

Figure 10. Heat release rate presented as functions of core gas temperature for RD5-87 and the four surrogates at ϕ = 0.4, 21% O_2, Pc = 40 bar and Tc = 900 K. (a) experimental results; (b) simulation results. The results for RD5-87 in both plots (solid green lines) are experimental results.

4.3. Sensitivity analysis

To draw further insight into surrogate-to-surrogate differences, brute force sensitivity analysis is conducted on the main ignition delay time using constant volume simulations for the four surrogates at Tc = 760 K / Pc = 40 bar and Tc = 900 K / Pc = 25 bar that are representative of boosted/low-temperature, and naturally aspirated combustion in HCCI engines, respectively. The sensitivity coefficients are defined as $S_{rel} = \ln\left(\frac{\tau^{\Delta}}{\tau}\right)/\ln\left(\frac{k^{\Delta}}{k}\right)$, where τ^{Δ} is the main ignition delay time after multiplying the original rate constant by 2, i.e., $k^{\Delta} = 2 * k$, and τ is the original ignition delay time. Negative sensitivity coefficients indicate that the reaction promotes reactivity, while positive coefficients indicate an inhibiting effect. Figure 11 presents the computed sensitivities for the 20 most sensitive reactions for the four surrogates. The species participating in these reactions are identified in the species dictionary in the Supplementary Material, with the molecular structures shown in Table S2.

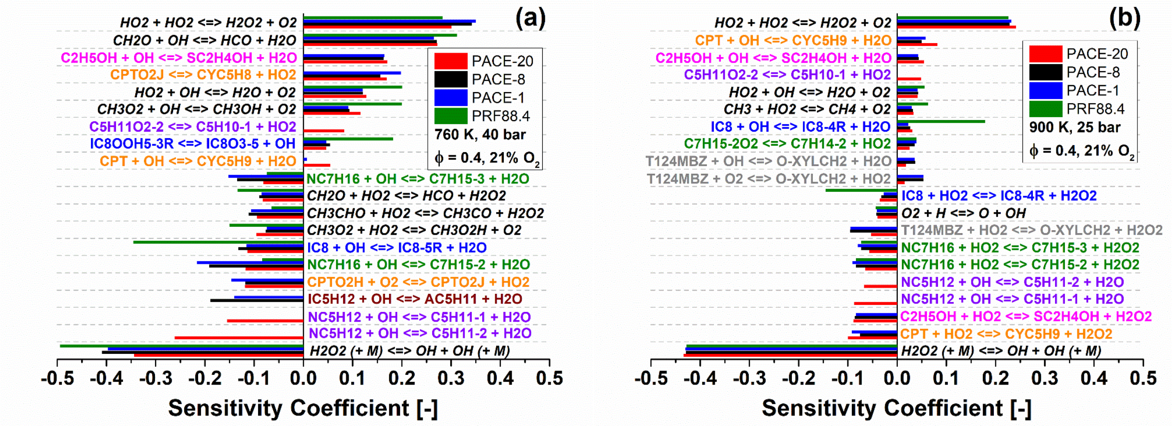

Figure 11. Sensitivity analysis on main ignition delay time for PACE-20, PACE-8, PACE-1 and PRF88.4 at (a) Tc = 760 K and Pc = 40 bar and (b) Tc = 900 K and Pc = 25 bar. Colored reactions are fuel-specific reactions from various sub-chemistries, while reactions in black and italic are non-fuel-specific reactions that can be contributed by various sub-chemistries. Negative coefficients indicate an inhibiting effect, while positive coefficients indicate a promoting effect on ignition reactivity.

At Tc = 760 K and Pc = 40 bar (Fig. 11a), the reaction classes of major importance include HO_2 recombination, H_2O_2 decomposition, H-atom abstraction by OH radical from fuel molecules, concerted elimination of HO_2 from RO_2 radicals, and non-fuel specific chemistries related to CH_2O, CH_3O_2 and CH_3CHO. The most sensitive reactions for the three multi-component surrogates are dominated by the sub-chemistries of paraffinic components (both *n*- and *iso*-), cyclopentane and ethanol, with minor contributions from aromatics and 1-hexene sub-chemistries despite their significant concentrations in the multi-component surrogates (c.f. Table 1). Among all the surrogates, PACE-20 shows unique and great dependence on *n*-pentane-specific pathways, e.g., $NC_5H_{12}+OH=C_5H_{11}\text{-}2+H_2O$, $NC_5H_{12}+OH=C_5H_{11}\text{-}1+H_2O$ and $C_5H_{11}O_2\text{-}2=C_5H_{10}\text{-}1+HO_2$, which dominate over the other sub-chemistries. These pathways are not present for PACE-1 and PACE-8 since they do not contain *n*-pentane. *iso*-Pentane, which is included in PACE-1 and PACE-8 but not in PACE-20, contributes to PACE-1 and PACE-8 reactivity, e.g., via $IC_5H_{12}+OH=AC_5H_{11}+H_2O$. However, the promoting effect from *iso*-pentane pathways is not as strong as *n*-pentane has on PACE-20, as can be inferred from Fig. 11a. These trends agree with the simulation results in Figs. 6a and 8 where PACE-20 is the most reactive among all surrogates. Sufficient characterization of the kinetics related to these pathways is necessary to address the inconsistency between the model and experiments shown in Fig. 6a. Also seen in Fig. 11a is the considerably increased sensitivity for $CPT+OH=CYC_5H_9+H_2O$ for PACE-20, which has negligible contribution for PACE-1 and PACE-8, though the concentration of cyclopentane is similar in the three multi-component surrogates. The cause for this is not immediately clear, which could be related to the interference from *n*-pentane sub-chemistry, where *n*-pentane initiates rapid OH branching at a faster rate and an earlier timing for PACE-20 than *iso*-pentane does for PACE-1 and PACE-8. The earlier onset of OH production will facilitate the cyclopentane consumption via the H-atom abstraction by OH radicals, making it more sensitive for PACE-20. Sufficiently characterizing the chemical kinetics of *n*-pentane and their impact on other fuel components are important for replicating RD5-87 since *n*-pentane is a major component in RD5-87, i.e., RD5-87 contains 8.8% of *n*-pentane on liquid volume basis, as seen in Table 1. While *iso*-pentane is considerably used to formulate PACE-1 and PACE-8, it has negligible concentration in RD5-87 (i.e., <0.1% on liquid volume basis). These results indicate that PACE-20 represents better the chemistry of RD5-87 than PACE-1 and PACE-8, particularly in those related to *n*-pentane and *iso*-pentane that are sensitive to autoignition reactivity. Differences between PACE-20 and the other two multi-component surrogates are also observed in *n*-heptane pathways (e.g., $NC_7H_{16}+OH=C_7H_{15}$-2+H_2O and $NC_7H_{16}+OH=C_7H_{15}$-3+H_2O), where the sensitivities of these pathways for PACE-20 are about 60% of that for PACE-1 and PACE-8. This is expected since *n*-heptane concentration in PACE-20 is much lower than those in PACE-1 and PACE-8. Additionally, *n*-heptane is the only *n*-paraffin in PACE-1 and PACE-8, and provides low temperature reactivity for these surrogates. PRF88.4 differs from the multi-component surrogates primarily in the pathways from iso-octane sub-chemistry, which display considerably higher sensitivities due to the higher iso-octane concentration in PRF88.4.

At Tc = 900 K and Pc = 25 bar (Fig. 11b), the magnitude of sensitivity coefficients is reduced for many reactions compared to Fig. 11a, with HO_2 recombination and H_2O_2 decomposition remaining the top inhibiting and promoting pathways, respectively. There is also an obvious shift in the most sensitive reactions from H-atom abstractions by OH toward abstractions by HO_2. Despite this, the H-atom abstraction pathways by OH from *n*-pentane are still among the top sensitive reactions for PACE-20, while that from *iso*-pentane for PACE-1 and PACE-8 that is observed in Fig. 11a does not show among the 20 most sensitive reactions. This, again, aligns well with the simulation results in Fig. 6b where the model predicts the highest reactivity for PACE-20.

4.4. Rate of production analysis

Rate of production (ROP) analysis is carried out for OH and HO_2 radicals at 5% iso-octane consumption for the four surrogates at the same conditions as in Fig. 11. The results for OH and HO_2 are summarized in Figs. 12 and 13, respectively, with the 20 most dominant pathways presented.

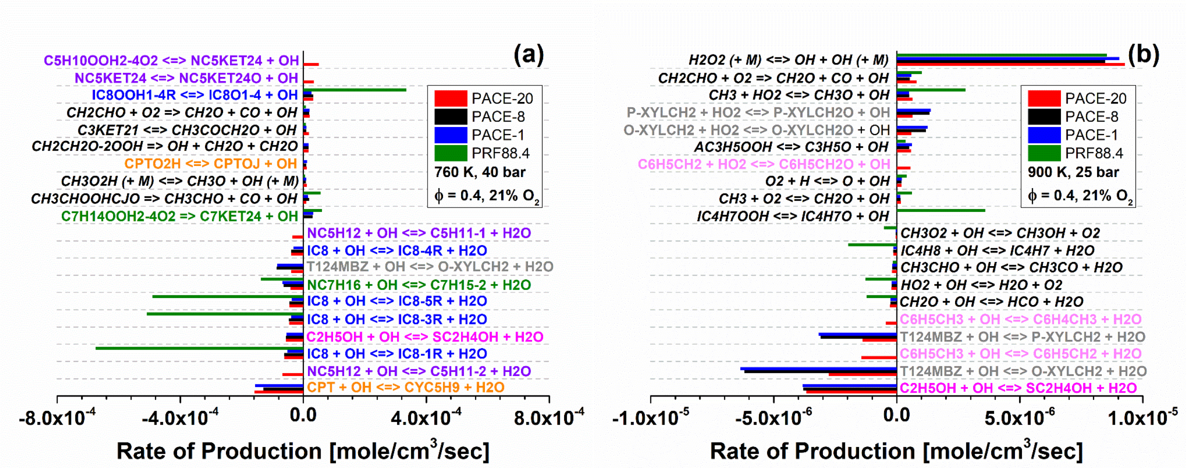

Figure 12. ROP analysis of OH for PACE-20, PACE-8, PACE-1 and PRF88.4 at (a) Tc = 760 K and Pc = 40 bar and (b) Tc = 900 K and Pc = 25 bar, at 5% iso-octane consumption. Colored reactions are fuel-specific reactions from various sub-chemistries, while reactions in black and italic are non-fuel-specific reactions that can be contributed by various sub-chemistries.

At Tc = 760 K and Pc = 40 bar (Fig. 12 a), OH radical is primarily produced from cyclization of QOOH radials yielding cyclic ethers. The produced OH radicals are almost completely consumed via H-atom abstractions from parent fuels. At this stage (i.e., 5% *iso*-octane consumption), OH production is largely promoted by *n*-pentane for PACE-20 (i.e., the top two OH producing pathways are from *n*-pentane sub-chemistry), and by *iso*-octane for PRF88.4, leading to their higher reactivity compared to PACE-1 and PACE-8, as already seen in Figs. 6a and 8. The produced OH radicals are primarily consumed via CPT+OH=CYC_5H_9+H_2O for the multi-component surrogates, and via IC_8+OH pathways for PRF88.4. Additional and unique contributions from NC_5H_{12}+OH pathways are also observed for PACE-20, which further increase PACE-20 reactivity given the promoting effect of these reactions, as shown in Fig. 11a. These findings support the conjectures made earlier with Fig. 11; that is, *n*-pentane in PACE-20 facilitates OH production at early stages of oxidation process than *iso*-pentane does for PACE-1 and PACE-8, which promotes the consumption of other fuel components (e.g., cyclopentane) and leads to increased fuel reactivity for PACE-20 in comparison to the others. In order to confirm this, simulated mole fractions for the fuel components of PACE-1, PACE-8 and PACE-20 at Tc = 760 K and Pc = 40 bar are shown in Fig. S5 in the Supplementary Material. It is seen that fuel consumption follows *n*-heptane > *1*-hexene > cyclopentane > *n*-pentane or *iso*-pentane > aromatics & ethanol. For PACE-20, the consumption rate for *n*-pentane is faster than *iso*-pentane for PACE-1 and PACE-8. Also seen in Fig. S5 is that tetralin has the fastest consumption rate among all fuel components for PACE-20. Nevertheless, both SA and ROP analysis indicate that it contributes insignificantly to the surrogate-to-surrogate differences in fuel reactivity.

At Tc = 900 K and Pc = 25 bar (Fig. 12b), OH production and consumption are less significant compared to those in Fig. 12a, as can be told from the magnitude of ROP. This is due primarily to the reduced fuel reactivity at this condition (e.g., Fig. 8 indicates τ is ~10 ms at 760 K and 40 bar vs. ~18 ms at 900 K and 25 bar for PACE-20). At this condition, OH production is mostly contributed by H_2O_2 decomposition, differing from that observed in Fig. 12a, while OH consumption is dominated by H-atom abstraction reactions from ethanol and aromatics, other than *iso*-octane and cyclopentane that are observed at Tc = 760 K and 40 bar. The ROPs are similar between PACE-1, PACE-8 and PACE-20, while the rate of consumption via aromatics are somewhat lower for PACE-20, leading to a greater net OH ROP, hence higher fuel reactivity, for PACE-20 than PACE-1 and PACE-8. This is consistent with the trends inferred from the simulation results presented in Figs. 7 and 8. The rate of consumption via aromatics is higher for PACE-1 and PACE-8 because of they contain more 1,2,4-trimethylbenzene which has 9 allylic H-atoms that are easily extracted by OH.

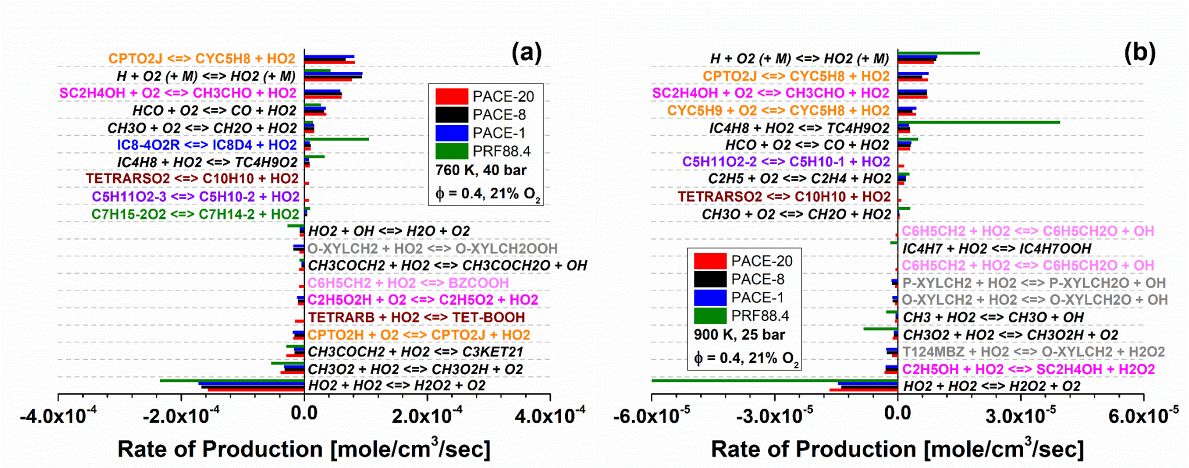

Figure 13. ROP analysis of HO_2 for PACE-20, PACE-8, PACE-1 and PRF88.4 at (a) Tc = 760 K and Pc = 40 bar and (b) Tc = 900 K and Pc = 25 bar, at 5% iso-octane consumption. Colored reactions are fuel-specific reactions from various sub-chemistries, while reactions in black and italic are non-fuel-specific reactions that can be contributed by various sub-chemistries.

For HO_2 (Fig. 13), at both conditions HO_2 radical is primarily produced via $H+O_2(+M)=HO_2(+M)$ for all surrogates as well as from cyclopentane and ethanol pathways for the multi-component surrogates, and consumed mostly via $HO_2+HO_2=H_2O_2+O_2$. The contribution from non-fuel specific reactions to HO_2 production and consumption is greater than that observed for OH radicals, which greatly complicates the kinetic interpretation of surrogate-to-surrogate difference since the non-fuel-specific species involved can be produced from various surrogates. For instance, $CH_3O_2+HO_2=CH_3O_2H+O_2$ is the second and fourth important HO_2 consuming pathway in Fig. 13a and 13b, where the CH_3O_2 radical can be produced from all fuel components. It is challenging to distinguish the contribution from each fuel component to this consuming pathway due to the intertwined non-fuel specific chemistry. Using the molecular tagging approach developed by Cheng et al. [66, 68] could help elucidate this, but this is beyond the scope of the current study. Despite this, it is clear from Fig. 13 that tetralin-specific pathways contribute uniquely to PACE-20 in HO_2 production and consumption. These pathways lead to the production of QOOH, and HO_2 radical that further undergoes HO_2 recombination to form H_2O_2, which both result in OH production that facilitate fuel reactivity. The large production of HO_2 derived from cyclopentane and ethanol ($CPTO_2J$ and SC_2H_4OH) is remarkable because these surrogate components comprise < 20% of the PACE surrogates.

5. SUMMARY AND CONCLUSIONS

To characterize the surrogate fidelity needed to replicate the complex autoignition behavior exhibited within advanced combustion engines, and specifically gasoline HCCI, autoignition and preliminary heat release behavior of RD5-87 are compared with its surrogates (namely PACE-1, PACE-8, PACE-20 and PRF88.4). The Sandia LTGC research engine is employed under fully-premixed HCCI-like conditions at Pin = 1.0 bar (naturally aspirated conditions) and Pin = 2.0 bar (high-boost conditions), with the ANL tpRCM used at a lean/undiluted fuel loading, compressed temperatures from 680 to 955 K, and compressed pressures at 15, 25, 40 and 60 bar. A recently updated gasoline surrogate model is also utilized to perform chemical kinetic modeling and to generate kinetic insights into the surrogate-to-surrogate differences. Comprehensive analyses of the experimental and modeling results indicate the following:

- Both the naturally aspirated and boosted engine experiments show that, in comparison to RD5-87, PACE-20 displays nearly identical ignition characteristics, whereas faster phasing is observed for PACE-1 and PACE-8. Heat release analysis indicates that the higher reactivity of PACE-1 and PACE-8 corresponds to their stronger ITHR and LTHR at naturally aspirated and boosted conditions, respectively.

- As with the LTGC engine results, the RCM experiments reveal that PACE-20 outperforms PACE-1, PACE-8 and PRF88.4 in replicating, both qualitatively and quantitatively, the typical low-temperature, NTC and intermediate-temperature autoignition behaviors, as well as the multi-stage heat release behavior for RD5-87 at all pressures.
- Excellent mapping is observed between the tpRCM and LTGC engine, where the ignition regimes determined from RCM datasets correlate well with the engine pressure-temperature trajectories at both naturally aspirated and boosted conditions. Comparison of ignition isopleths in a P-T space shows that PACE-20 represents RD5-87 remarkably at all temperatures and pressures covering naturally aspirated/intermediate-temperature to high-boost/low-temperature engine operating regimes, whereas PACE-1, PACE-8 and PRF88.4 only represent RD5-87 sufficiently within the naturally aspirated/intermediate-temperature regime.
- The model performs excellently for PACE-20 in replicating both autoignition and preliminary heat release, while showing some inadequacies for PACE-1, PACE-8 and PRF88.4, with greater discrepancies observed at high-pressure and low-temperature/NTC conditions, indicating a need to further improve the model for its use in surrogate fuel design.
- Sensitivity and ROP analyses highlight surrogate-to-surrogate differences in the controlling chemical kinetics, and indicate that the higher reactivity of PACE-20 than the other surrogates is attributed to its higher concentration of *n*-alkanes,

where *n*-pentane initiates rapid OH branching at a faster rate and an earlier timing for PACE-20 than *iso*-pentane does for PACE-1 and PACE-8. This trend is opposite to that observed in the test measurements.

It is obvious from both the LTGC engine and tpRCM experiments that the performance of the surrogates follows the order of PACE-20 > PACE-1 > PACE-8 > PRF88.4, even though all the surrogates reproduce the AKI of RD5-87 within the standard octane rating tolerance. Also important is that the better match in RON, MON and S for PACE-8 compared to PACE-1 does not lead to improved surrogate performance for PACE-8, but instead somewhat deteriorated performance at low temperatures that can be more relevant to HCCI combustion.

The observations made in this work reiterate the insufficiency of standardized properties (i.e., RON, MON and S) to properly represent fuel behavior in advanced combustion schemes such as HCCI where complex autoignition pathways play an important role in initiating or propagating the combustion process, and call for better surrogate formulation methodologies that implement improved fuel metrics for the formulation of high-fidelity surrogates. This finding is applicable to other combustion systems, such as advanced gas turbines where low-, NTC and intermediate temperature chemical kinetics can affect ignition, flame stabilization and blowout. The commendable surrogate fidelity of PACE-20, as opposed to PACE-1, PACE-8 and PRF88.4, in replicating both LTHR and autoignition characteristics of RD5-87 at all conditions investigated in this study serves as a successful demonstration of such implementation, where lean/HCCI-like autoignition characteristics are tailored and incorporated, complementing the standardized properties, as additional target properties for surrogate formulation.

6. ACKNOWLEDGEMENT

This manuscript has been created by UChicago Argonne, LLC, Operator of Argonne National Laboratory, a U.S. Department of Energy Office of Science laboratory, under Contract No. DE-AC02-06CH11357. The work at LLNL was performed under the auspices of the U.S. Department of Energy (DOE), Contract DE-AC52-07NA27344. The work at SNL was performed under the auspices of the U.S. Department of Energy (DOE), Contract DE-NA0003525. The U.S. Government retains for itself, and others acting on its behalf, a paid-up nonexclusive, irrevocable worldwide license in said article to reproduce, prepare derivative works, distribute copies to the public, and perform publicly and display publicly, by or on behalf of the Government. The DOE will provide public access in accordance with http://energy.gov/downloads/doe-public-access-plan.

This research was conducted as part of the Partnership to Advance Combustion Engines (PACE) sponsored by the U.S. Department of Energy (DOE) Vehicle Technologies Office (VTO), and the Co-Optimization of Fuels and Engines (Co-Optima) initiative sponsored by the U.S. DOE Office of Energy Efficiency and Renewable Energy and Bioenergy Technologies, and VTO. Co-Optima is a collaborative project of multiple national laboratories initiated to simultaneously accelerate the introduction of affordable, scalable, and sustainable biofuels and high-efficiency, low-emission vehicle engines. Special thanks to program managers Kevin Stork, Gurpreet Singh, and Mike Weismiller.

The authors would like to acknowledge Dr. Jeffrey Santner, Dr. Toby Rockstroh, Dr. Dongil Kang and Mr. Jason Bromberek for their efforts to maintain ANL’s tpRCM. The authors would also like to thank Tim Gilbertson, Keith Penney, Aaron Czeszynski and Alberto Garcia for their dedicated support of the LTGC Engine Laboratory.

7. REFERENCE

[1] Annual energy outlook 2021, Energy Information Administration, Washington, DC, 2021.

[2] S.M. Sarathy, A. Farooq, G.T. Kalghatgi, Recent progress in gasoline surrogate fuels, Progress in Energy and Combustion Science 65 (2018) 67-108.

[3] W.J. Pitz, C.J. Mueller, Recent progress in the development of diesel surrogate fuels, Progress in Energy and Combustion Science 37 (2011) 330-350.

[4] ASTM International, Standard Test Method for Research Octane Number of Spark-Ignition Engine Fuel, ASTM West Conshohocken, PA, D2699, 2007.

[5] ASTM International, Standard Test Method for Motor Octane Number of Spark-Ignition Engine Fuel, ASTM West Conshohocken, PA, D2700, 2013.

[6] J.C.G. Andrae, Development of a detailed kinetic model for gasoline surrogate fuels, Fuel 87 (2008) 2013-2022.

[7] J.C.G. Andrae, P. Björnbom, R.F. Cracknell, G.T. Kalghatgi, Autoignition of toluene reference fuels at high pressures modeled with detailed chemical kinetics, Combustion and Flame 149 (2007) 2-24.

[8] C. Pera, V. Knop, Methodology to define gasoline surrogates dedicated to auto-ignition in engines, Fuel 96 (2012) 59-69.

[9] M. Mehl, J.Y. Chen, W.J. Pitz, S.M. Sarathy, C.K. Westbrook, An Approach for Formulating Surrogates for Gasoline with Application toward a Reduced Surrogate Mechanism for CFD Engine Modeling, Energy Fuels 25 (2011) 5215-5223.

[10] A. Ahmed, G. Goteng, V.S.B. Shankar, K. Al-Qurashi, W.L. Roberts, S.M. Sarathy, A computational methodology for formulating gasoline surrogate fuels with accurate physical and chemical kinetic properties, Fuel 143 (2015) 290-300.

[11] O.S. Abianeh, M.A. Oehlschlaeger, C.-J. Sung, A surrogate mixture and kinetic mechanism for emulating the evaporation and autoignition characteristics of gasoline fuel, Combustion and Flame 162 (2015) 3773-3784.

[12] S. Cheng, C. Saggese, D. Kang, S.S. Goldsborough, S.W. Wagnon, G. Kukkadapu, K. Zhang, M. Mehl, W.J. Pitz, Autoignition and preliminary heat release of gasoline surrogates and their blends with ethanol at engine-relevant conditions: Experiments and comprehensive kinetic modeling, Combustion and Flame 228 (2021) 57-77.

[13] S. Cheng, D. Kang, A. Fridlyand, S.S. Goldsborough, C. Saggese, S. Wagnon, M.J. McNenly, M. Mehl, W.J. Pitz, D. Vuilleumier, Autoignition behavior of gasoline/ethanol blends at engine-relevant conditions, Combustion and Flame 216 (2020) 369-384.

[14] S.S. Goldsborough, J. Santner, D. Kang, A. Fridlyand, T. Rockstroh, M.C. Jespersen, Heat release analysis for rapid compression machines: Challenges and opportunities, Proceedings of the Combustion Institute 37 (2019) 603-611.

[15] G. Kalghatgi, Fuel anti-knock quality-Part I. Engine studies, SAE Transactions (2001) 1993-2004.

[16] I. Truedsson, M. Tuner, B. Johansson, W. Cannella, Pressure Sensitivity of HCCI Auto-Ignition Temperature for Gasoline Surrogate Fuels, Report No. 0148-7191, SAE Technical Paper 2013-01-1669, 2013.

[17] I. Truedsson, M. Tuner, B. Johansson, W. Cannella, Pressure sensitivity of HCCI auto-ignition temperature for oxygenated reference fuels, Journal of Engineering for Gas Turbines and Power 135 (2013).

[18] I. Truedsson, M. Tuner, B. Johansson, W. Cannella, Pressure sensitivity of HCCI auto-ignition temperature for primary reference fuels, SAE International Journal of Engines 5 (2012) 1089-1108.

[19] J. Lacey, K. Kameshwaran, S. Sathasivam, Z. Filipi, W. Cannella, P.A. Fuentes-Afflick, Effects of refinery stream gasoline property variation on the auto-ignition quality of a fuel and homogeneous charge compression ignition combustion, International Journal of Engine Research 18 (2017) 226-239.

[20] A. Krisman, E.R. Hawkes, J.H. Chen, A parametric study of ignition dynamics at ECN Spray A thermochemical conditions using 2D DNS, Proceedings of the Combustion Institute 37 (2019) 4787-4795.

[21] V.N. Parmon, G.I. Panov, A. Uriarte, A.S. Noskov, Nitrous oxide in oxidation chemistry and catalysis: application and production, Catalysis Today 100 (2005) 115-131.

[22] S. Wagnon, Development of an Optimized Gasoline Surrogate Formulation for PACE Experiments and Simulations, Advanced Engine and Fuel Technologies 2020 Annual Progress Report (2021).

[23] J.E. Dec, J. Dernotte, C. Ji, Increasing the Load Range, Load-to-Boost Ratio, and Efficiency of Low-Temperature Gasoline Combustion (LTGC) Engines, SAE International Journal of Engines 10 (2017) 1256-1274.

[24] D. Lopez-Pintor, J.E. Dec, Experimental Evaluation of a Gasoline-like Fuel Blend with High Renewable Content to Simultaneously Increase ϕ-Sensitivity, RON, and Octane Sensitivity, Energy & Fuels 35 (2021) 16482-16493.

[25] D.L. Pintor, J. Dec, G. Gentz, Experimental Evaluation of a Custom Gasoline-Like Blend Designed to Simultaneously Improve φ-Sensitivity, RON and Octane Sensitivity, SAE International Journal of Advances Current Practices in Mobility 2 (2020) 2196-2216.

[26] D.L. Pintor, J. Dec, G. Gentz, ϕ-sensitivity for LTGC engines: Understanding the fundamentals and tailoring fuel blends to maximize this property, SAE Technical Paper 2019-01-0961, 2019.

[27] D. Vuilleumier, X. Huan, T. Casey, M. Sjöberg, Uncertainty Assessment of Octane Index Framework for Stoichiometric Knock Limits of Co-Optima Gasoline Fuel Blends, SAE International Journal of Fuels and Lubricants 11 (2018) 247-270.

[28] J. Szybist, Knock Mitigation Effectiveness of EGR across the Pressure-Temperature Domain, SAE International Journal of Advances and Current Practices in Mobility 3 (2020) 262-275.

[29] B.P. Maldonado, B.C. Kaul, C.D. Schuman, S.R. Young, J.P. Mitchell, Next-Cycle Optimal Fuel Control for Cycle-to-Cycle Variability Reduction in EGR-Diluted Combustion, IEEE Control Systems Letters 5 (2021) 2204-2209.

[30] J. Pulpeiro González, C.M. Hall, C.P. Kolodziej, Determination of a most representative cycle from cylinder pressure ensembles via statistical method using distribution skewness, International Journal of Engine Research (2021) doi:10.1177/14680874211065525.

[31] Q. Peng, T. Rockstroh, C. Hall, The impact of fuel and injection strategy on combustion characteristics, emissions and efficiency in gasoline compression ignition operation, Fuel 318 (2022) 123548.

[32] A. Cuoci, C.T. Avedisian, J.D. Brunson, S. Guo, A. Dalili, Y. Wang, M. Mehl, A. Frassoldati, K. Seshadri, J.E. Dec, D. Lopez-Pintor, Simulating combustion of a seven-component surrogate for a gasoline/ethanol blend including soot formation and comparison with experiments, Fuel 288 (2021) 119451.

[33] K.C. Kalvakala, P. Pal, J.P. Gonzalez, C.P. Kolodziej, H.J. Seong, G. Kukkadapu, M. McNenly, S. Wagnon, R. Whitesides, N. Hansen, S.K. Aggarwal, Numerical analysis of soot emissions from gasoline-ethanol and gasoline-butanol blends under gasoline compression ignition conditions, Fuel 319 (2022) 123740.

[34] G. Guleria, D. Lopez-Pintor, J.E. Dec, D. Assanis, A comparative study of gasoline skeletal mechanisms under partial fuel stratification conditions using large eddy simulations, International Journal of Engine Research (2021) doi:10.1177/14680874211031370.

[35] K. Wan, J. Manin, H.S. Sim, I. Karathanassis, Soot and PAH formation in high pressure spray pyrolysis of gasoline and diesel fuels, Combustion and Flame 241 (2022) 112084.

[36] ASTM D86, Standard Test Method for Distillation of Petroleum Products and Liquid Fuels at Atmospheric Pressure, ASTM International, West Conshohocken, PA, 2020.

[37] P. Pal, K. Kalvakala, Y. Wu, M. McNenly, S. Lapointe, R. Whitesides, T. Lu, S.K. Aggarwal, S. Som, Numerical Investigation of a Central Fuel Property Hypothesis Under Boosted Spark-Ignition Conditions, Journal of Energy Resources Technology 143 (2020).

[38] J. Mueller, N. Kim, S. Lapointe, M.J. McNenly, M. Sjöberg, R. Whitesides, Chapter 2 - Optimization of fuel formulation using adaptive learning and artificial intelligence, in: J. Badra, P. Pal, Y. Pei, S. Som (Eds.), Artificial Intelligence and Data Driven Optimization of Internal Combustion Engines, Elsevier 2022, pp. 27-45.

[39] S.M. Sarathy, G. Kukkadapu, M. Mehl, T. Javed, A. Ahmed, N. Naser, A. Tekawade, G. Kosiba, M. AlAbbad, E. Singh, S. Park, M.A. Rashidi, S.H. Chung, W.L. Roberts, M.A. Oehlschlaeger, C.-

J. Sung, A. Farooq, Compositional effects on the ignition of FACE gasolines, Combustion and Flame 169 (2016) 171-193.

[40] E. Lemmon, I.H. Bell, M. Huber, M. McLinden, NIST Standard Reference Database 23: Reference Fluid Thermodynamic and Transport Properties-REFPROP, Version 10.0, National Institute of Standards and Technology, Standard Reference Data Program, Gaithersburg, 2018.

[41] K. Aikawa, T. Sakurai, J.J. Jetter, Development of a Predictive Model for Gasoline Vehicle Particulate Matter Emissions, SAE International Journal of Fuels and Lubricants 3 (2010) 610-622.

[42] Yaws, Carl L Narasimhan, Prasad, K. Gabbula, Chaitanya. (2009). Yaws' Handbook of Antoine Coefficients for Vapor Pressure (2nd Electronic Edition). Knovel. Retrieved from https://app.knovel.com/hotlink/toc/id:kpYHACVPEH/yaws-handbook-antoine/yaws-handbook-antoine.

[43] Yaws, Carl L. (2008). Yaws' Handbook of Physical Properties for Hydrocarbons and Chemicals. Knovel. Retrieved from https://app.knovel.com/hotlink/toc/id:kpYHPPHC0B/yaws-handbook-physical/yaws-handbook-physical.

[44] C.K. Westbrook, M. Sjöberg, N.P. Cernansky, A new chemical kinetic method of determining RON and MON values for single component and multicomponent mixtures of engine fuels, Combustion and Flame 195 (2018) 50-62.

[45] S. Burke, R. Rhoads, M. Ratcliff, R. McCormick, B. Windom, Measured and predicted vapor liquid equilibrium of ethanol-gasoline fuels with insight on the influence of azeotrope interactions on aromatic species enrichment and particulate matter formation in spark ignition engines, Report No. 0148-7191, SAE Technical Paper 2018-01-03, 2018.

[46] J.E. Dec, Y. Yang, N. Dronniou, Boosted HCCI-controlling pressure-rise rates for performance improvements using partial fuel stratification with conventional gasoline, SAE International Journal of Engines 4 (2011) 1169-1189.

[47] G. Gentz, J. Dernotte, C. Ji, J. Dec, Spark Assist for CA50 Control and Improved Robustness in a Premixed LTGC Engine–Effects of Equivalence Ratio and Intake Boost, Report No. 0148-7191, SAE Technical Paper, 2018.

[48] J.E. Dec, Y. Yang, Boosted HCCI for high power without engine knock and with ultra-low NOx emissions-using conventional gasoline, SAE International Journal of Engines 3 (2010) 750-767.

[49] Y. Yang, J. Dec, N. Dronniou, W. Cannella, Boosted HCCI combustion using low-octane gasoline with fully premixed and partially stratified charges, J SAE International Journal of Engines 5 (2012) 1075-1088.

[50] W. Hwang, J. Dec, M. Sjöberg, Spectroscopic and chemical-kinetic analysis of the phases of HCCI autoignition and combustion for single-and two-stage ignition fuels, Combustion and Flame 154 (2008) 387-409.

[51] J. Eng, Characterization of pressure waves in HCCI combustion, Report No. 0148-7191, SAE Technical Paper 2002-01-2859, 2002.

[52] J. Dernotte, J.E. Dec, C. Ji, Energy distribution analysis in boosted HCCI-like/LTGC engines-understanding the trade-offs to maximize the thermal efficiency, SAE International Journal of Engines 8 (2015) 956-980.

[53] J.E. Dec, M. Sjöberg, A parametric study of HCCI combustion—the sources of emissions at low loads and the effects of GDI fuel injection, SAE Transactions (2003) 1119-1141.

[54] J.B. Heywood, Internal combustion engine fundamentals, McGraw-Hill, New York, 1988.

[55] G. Woschni, A universally applicable equation for the instantaneous heat transfer coefficient in the internal combustion engine, Report No. 0148-7191, SAE Technical Paper 670931, 1967.

[56] Petitpas, G., Whitesides, R., Dernotte, J., and Dec, J., "Refining Measurement Uncertainties in HCCI/LTGC Engine Experiments," SAE Technical Paper 2018-01-1248, 2018.

[57] A. Fridlyand, S.S. Goldsborough, M. Al Rashidi, S.M. Sarathy, M. Mehl, W.J. Pitz, Low temperature autoignition of 5-membered ring naphthenes: Effects of substitution, Combustion and Flame 200 (2019) 387-404.

[58] T. Rockstroh, A. Fridlyand, S. Ciatti, W. Cannella, S.S. Goldsborough, Autoignition behavior of a full boiling-range gasoline: Observations in RCM and GCI engine environments, Combustion and Flame 209 (2019) 239-255.

[59] B.W. Weber, C.-J. Sung, M.W. Renfro, On the uncertainty of temperature estimation in a rapid compression machine, Combustion and Flame 162 (2015) 2518-2528.

[60] A. Fridlyand, M.S. Johnson, S.S. Goldsborough, R.H. West, M.J. McNenly, M. Mehl, W.J. Pitz, The role of correlations in uncertainty quantification of transportation relevant fuel models, Combustion and Flame 180 (2017) 239-249.

[61] S. Cheng, Y. Yang, M.J. Brear, M. Frenklach, Quantifying uncertainty in kinetic simulation of engine autoignition, Combustion and Flame 216 (2020) 174-184.

[62] Y. Li, C.-W. Zhou, K.P. Somers, K. Zhang, H.J. Curran, The oxidation of 2-butene: A high pressure ignition delay, kinetic modeling study and reactivity comparison with isobutene and 1-butene, Proceedings of the Combustion Institute 36 (2017) 403-411.

[63] C. Saggese, C.M. Thomas, S.W. Wagnon, G. Kukkadapu, S. Cheng, D. Kang, S.S. Goldsborough, W.J. Pitz, An improved detailed chemical kinetic model for C3-C4 linear and iso-alcohols and their blends with gasoline at engine-relevant conditions, Proceedings of the Combustion Institute 38 (2021) 415-423.

[64] S. Cheng, D. Kang, S.S. Goldsborough, C. Saggese, S. Wagnon, W.J. Pitz, Experimental and modeling study of C2-C4 alcohol autoignition at intermediate temperature conditions, Proceedings of the Combustion Institute 38 (2021) 709-717.

[65] S.S. Goldsborough, S. Cheng, D. Kang, C. Saggese, S. Wagnon, W.J. Pitz, Effects of isoalcohol blending with gasoline on autoignition behavior in a rapid compression machine: isopropanol and isobutanol, Proceedings of the Combustion Institute 38 (2021) 5655-5664.

[66] S. Cheng, S.S. Goldsborough, C. Saggese, S.W. Wagnon, W.J. Pitz, New insights into fuel blending effects: intermolecular chemical kinetic interactions affecting autoignition times and intermediate-temperature heat release, Combustion and Flame 233 (2021) 111559.

[67] M.J. McNenly, R.A. Whitesides, D.L. Flowers, Faster solvers for large kinetic mechanisms using adaptive preconditioners, Proceedings of the Combustion Institute 35 (2015) 581-587.

[68] S. Cheng, S.S. Goldsborough, S.W. Wagnon, W.J. Pitz, Probing intermediate temperature heat release in autoignition of C3-C4 iso-alcohol/gasoline blends, Combustion and Flame 233 (2021) 111602.

[69] K. Zhang, C. Banyon, J. Bugler, H.J. Curran, A. Rodriguez, O. Herbinet, F. Battin-Leclerc, C. B'Chir, K.A. Heufer, An updated experimental and kinetic modeling study of n-heptane oxidation, Combustion and Flame 172 (2016) 116-135.

[70] R. Fang, G. Kukkadapu, M. Wang, S.W. Wagnon, K. Zhang, M. Mehl, C.K. Westbrook, W.J. Pitz, C.-J. Sung, Fuel molecular structure effect on autoignition of highly branched iso-alkanes at low-to-intermediate temperatures: Iso-octane versus iso-dodecane, Combustion and Flame 214 (2020) 152-166.